Energy Reports 9 (2023) 4872–4892

Contents lists available at ScienceDirect

Energy Reports

journal homepage: www.elsevier.com/locate/egyr

Research paper

Novel integration between propane pre-cooled mixed refrigerant LNG process and concentrated solar power system based on supercritical CO_2 power cycle

Ahmad K. Sleiti, Wahib A. Al-Ammari, BSc. *

Department of Mechanical & Industrial Engineering, College of Engineering, Qatar University, Doha, Qatar

ARTICLE INFO

Article history:
Received 6 November 2022
Received in revised form 7 March 2023
Accepted 4 April 2023
Available online 15 April 2023

Keywords:
Propane pre-cooled mixed refrigerant (C3MR)
LNG
Concentrated solar power
Thermoeconomic analysis
Exergy analysis
Supercritical CO_2 power cycles

ABSTRACT

Liquefaction of natural gas (LNG) is an energy-intensive process with large CO_2 emissions. This study addresses these problems by introducing a novel hybrid integration between the propane pre-cooled mixed-refrigerant (C3MR) liquefaction process and concentrated solar power (CSP), utilizing an intercooled supercritical CO_2 power block. The proposed system is designed to minimize or eliminate the need for thermal energy storage (TES) and reduce CO_2 emissions while providing economic benefits. These benefits are obtained mainly by recovering the cold energy of the flash-gas of the C3MR process through the precooling process of the sCO_2 cycle. Then, the flash-gas is stored and combusted (using an auxiliary heater (AH)) at nighttime or when CSP is insufficient to meet the power demand. Five integration cases are evaluated from energetic, exergetic, economic, and environmental points of view: the sCO_2 cycle is driven by CSP and its thermal energy storage (TES) without AH in Case-1, by CSP+TES+AH in Case-2 to Case-4 with different contribution from TES and AH, and by CSP+AH without TES in Case-5. In addition, this study optimizes the operating parameters of the hybrid system to further enhance its economic and environmental benefits. The proposed system reduces the CSP field size, minimizes or eliminates the need for TES, and reduces or eliminates CO_2 emissions. The optimized results show that Case-2 and Case-5 reduced the levelized cost of electricity from 14.16¢/kWh to 10.35¢/kWh and 8.19¢/kWh, respectively, and reduced the CO_2 emissions by 86% and 36%. This study contributes to the field by introducing a novel hybrid integration between the C3MR process and CSP system, providing thorough evaluations of its performance and benefits, and providing significant benefits to the decarbonization strategies of LNG and other industrial processes.

1. Introduction

With the rapid growth of the worldwide energy demand, the natural gas (NG) demand is expected to increase by 1.6% per year (Zhang et al., 2020) in the coming decades. For transportation distances over 3500 km, the NG is exported as a liquefied NG (LNG) at −161 °C and atmospheric pressure as its volume is reduced by a factor of 600 (Sanavandi and Ziabasharhagh, 2016). Although NG is considered the cleanest fossil fuel, the energy-intensive LNG transportation chain is a major source of greenhouse gas (GHG) emissions. For instance, the LNG industry in the USA is projected to generate 130 to 213 million-metric-tons of new GHG emissions by 2030, equal to the annual emissions of 28 to 45 million fossil fuel-powered cars (Swanson et al., 2020). This is mainly owed to that the LNG chain consumes about 25% of the energy delivered. About 8% to 12% of this energy is consumed during the liquefaction process (Mackenzie, 2021). Therefore, several approaches were developed to improve the LNG processes by reducing their energy consumption, increasing their economic benefits, and minimizing their GHG emissions. These approaches can be introduced in five groups, which are: (1) modifying the structure or operating strategy of an existing LNG process, (2) integrating the LNG process with other thermal/chemical/electrical systems, (3) recovering the cold energy of the produced LNG using different techniques, (4) recovering the waste heat of their power drivers (gas turbines), and (5) optimizing the design and operation of an existing LNG process. A brief literature review of these approaches is presented in the next subsections.

According to the types of refrigerants and the number of refrigeration cycles, the LNG processes are classified into three groups: cascaded liquefaction process (three pure refrigerants in three refrigeration cycles) (Sun et al., 2022); mixed-refrigerant (MR) based process (single mixed-refrigerant (SMR), dual mixed-refrigerant (DMR), and propane pre-cooled mixed-refrigerant (C3MR)) (Sun et al., 2022); and N_2 expander-based processes

* Corresponding author.
E-mail address: wahib.alammari@qu.edu.qa (W.A. Al-Ammari).

https://doi.org/10.1016/j.egyr.2023.04.012

Nomenclature

Symbol

A	Heat transfer area (m^2)
DNI	Direct normal irradiance (W/m^2)
D	Diameter (m)
$\dot{E}$	Exergy rate (kW)
h	Specific enthalpy (kJ/kg) or Heat transfer coefficient (kW/m^2-°C)
k	Thermal conductivity (kW/m-°C)
l	Length (m)
$\dot{m}$	Mass flow rate (kg/s)
N	Number of tubes in the receiver
P	Pressure (bar) or Net output power (MW)
Q	Heat transfer rate (kW)
T	Temperature (°C)
$\dot{W}$	Work produced or consumed by a component (kW)
Z	Component cost ($)
η	Energy or exergy efficiency (%)
φ	Specific exergy (kJ/kg)

Subscripts

fg	Flash-gas
hel	Heliostat
heater	Heater of the sCO_2 power cycle
I,sCO_2	For energy efficiency of the sCO_2 cycle
I,CSP	For energy efficiency of the CSP field
II,sCO_2	For exergy efficiency of the sCO_2 cycle

Abbreviations

ARC	Absorption refrigeration cycle
CSP	Concentrated solar power
CST	Cold-salt tank
C3MR	Propane pre-cooled mixed-refrigerant process
DMR	Dual mixed-refrigerant process
GHG	Greenhouse gases
HTR	High temperature recuperator
HST	Hot-salt tank
LNG	Liquefaction of the NG
LTR	Low temperature recuperator
LCOE	Levelized cost of electricity
LHV	Lower heating value
MCFC	Molten carbonate fuel cell
MTPA	Million Tonnes Per Annum
MC	Main compressor
MR	Mixed refrigerant
NG	NG
ORC	Organic Rankine cycle
PC	Precooler
RC	Recompressor
SMR	Single mixed refrigerant
SOFC	Solid oxide fuel cell
SPT	Solar power tower system
SRC	Steam Rankine cycle
sCO_2	Supercritical carbon dioxide
TES	Thermal energy storage

(Lee et al., 2018). The MR processes are more attractive as they form an optimal solution for onshore and offshore applications on either large or small scales. The MR processes offer an optimal solution for both onshore and offshore applications making them highly attractive (Al-Mutaz et al., 2016). In particular, the C3MR process has lower specific energy consumption by an average of 10% compared to the cascaded process and 55% compared to the N_2 expander-based processes (Furda et al., 2022). However, the energy consumption of these process is relatively high and need to be reduced significantly to improve their economic benefits and mitigate their negative environmental impacts. Therefore, several studies attempt to enhance their energy performances by implementing some modifications to the existing MR processes. Bin Omar et al. (2014) proposed a novel MR-LNG process (MR-X) that combines the advantages of C3MR, DMR, and AP-X (designed by Air Products & Chemicals, Inc.) LNG processes. It consists of two MR blocks for precooling and liquefaction and a third N_2 block for subcooling. However, it has a complex structure and needs further research to improve its performance from economic and environmental viewpoints. As an alternative for large-scale LNG production, Almeida-Trasvina and Smith (2018) presented a novel cascaded MR cycle similar to the DMR cycle, called the CryoMan process. This process was developed at the University of Manchester specifically for small-scale LNG production (Almeida Trasviña, 2016). The novel CryoMan cascaded cycle achieved 5% energy savings compared to the basic DMR cycle. However, this comes at the cost of an increase in complexity and associated capital costs compared to the DMR cycle. Qyyum et al. (2020) proposed dual-effect single-mixed refrigeration (DSMR) cycle as an alternative to SMR and DMR cycles. The DSMR has a dual-effect configuration (similar to DMR) but uses only a single mixed-refrigerant (similar to SMR). Compared to the DMR, the authors reported that the DSMR achieves 22.89% energy savings with specific energy consumption of 0.284 kWh/kg-NG. Other modifications of LNG cycles were proposed using new propane- (Mazyan et al., 2020) and ammonia-based (Cycle et al., 2021) refrigerant blends for the precooling process in MR and N_2 expander cycles (Jin et al., 2022). These blends reduce the global warming potential by up to 24% and increase the COP by an average of 0.62 compared to the MR without ammonia.

Despite the improvements achieved by enhancing the cycles of LNG processes, the liquefaction of natural gas remains highly energy-intensive and a significant contributor to greenhouse gas emissions. Estimated CO_2 emissions associated with the LNG process account for approximately 6% to 10% of overall GHG emissions of the entire LNG value chain which underscores the need for more sustainable approaches to LNG production (Zhang and Saeid, 2022). While technologies such as Carbon Capture and Storage (CCS) and renewable energy integration (Sun et al., 2021) can potentially reduce the emissions from LNG production, significant progress is still required to achieve large-scale adoption and deployment of these technologies in the LNG industry (Rajabloo et al., 2023). In this respect, the integration of the LNG processes with cleaner energy sources and refrigeration systems is suggested in the literature. For example, the absorption refrigeration cycle (ARC) is proposed for the precooling process in the liquefaction plant (Mehrpooya et al., 2016; Ansarinasab and Mehrpooya, 2017; Zaitsev et al., 2020). Other researchers proposed the integration of solid oxide or molten carbonate fuel cells to generate the power for the liquefaction compressors and utilize their waste heat to drive an ARC for the precooling process of the LNG process (Shazed et al., 2021; Mehrpooya et al., 2021). But, the economic feasibility of these studies was not investigated. Recently, Afrouzy and Taghavi (2021) proposed solar energy to drive the DMR process, coupled with the Kalina power cycle driven by the waste heat of the compressors, using

photovoltaic (PV) panels. However, PV-based energy seems to be economical only for small-scale LNG production (less than 1 MTPA (Million-Tonnes-Per-Annum)).

Recovery of the cold energy of the flash-gas at the end of the LNG process is proposed to reduce the cold duty of its heat exchangers. Lim et al. (2014) analyzed several configurations to use the cold energy of the flash-gas within the SMR, C3MR, and N_2 expander processes. Although these configurations increase the complexity of the heat exchanger designs, they reported that some configurations reduce the specific work of the compressors by 4%–5%. Instead of the flash-gas, the recovery of the cold energy of the LNG at the regasification stage to be used in the liquefaction stage (using liquid air as a cold carrier) is introduced by Park et al. (2021). The extra capital expenditure could be recovered within two years via the reduction in annual operating costs. However, the recovery of the LNG cold energy at the regasification stage has more economic benefits and is more practical if performed near power plants rather than transforming liquid air to the exporting terminal of the LNG (Ghorbani et al., 2021). The cold energy of the LNG is used as a heat sink for oxy-fuel power plants and organic Rankine cycle (ORC) that utilizes CO_2 as a working fluid as investigated by Xiang et al. (2019), and Xia et al. (2019).

For ORC, the use of LNG as a heat sink makes it possible to generate power with low-grade heat sources even using the ambient air as in Xia et al. (2019). For the oxy-fuel cycle, the cold energy recovery of LNG through the condensation process reduces the cooling load of the precoolers and intercoolers of the plant. Also, it could be used to liquefy the exported CO_2 to be transported as a liquid to the market rather than as a compressed gas (Xiang et al., 2019). This saves additional compression power and is more practical than compression as only a small amount of CO_2 is exported in oxy-fuel-based sCO_2 power cycles. Simpler improvement for the LNG processes was introduced by the recovery of the waste heat from the flue gases of gas turbines (He and Lin, 2020). This heat is used to drive organic Rankine or absorption refrigeration cycles. To enhance the performance of the LNG process without increasing the complexity of the cycle or adding extra expenditures, optimizing the operation of the process to minimize the specific work of the plant must be applied. Therefore, several optimization studies were conducted for SMR (Santos et al., 2021), DMR (He and Lin, 2021; Wang et al., 2014), C3MR (Primabudi et al., 2019; Allahyarzadeh-Bidgoli et al., 2020), AP-X (Sun et al., 2016), and N_2 expander processes (Xiong et al., 2016).

Overviewing the aforementioned approaches, these improvements are mainly focused on the LNG process with no enhancement for the cycle drivers (mostly gas turbines) or investigations of feasible alternatives. Furthermore, these improvements only slightly decrease the CO_2 emissions and, in most cases, CO_2 emissions are not evaluated (see references Bin Omar et al. (2014), Almeida-Trasvina and Smith (2018), and Qyyum et al. (2020) as examples. In addition, the integration between solar-based power sources and LNG systems that utilizes PV panels as a power source is limited to small-scale LNG plants (Afrouzy and Taghavi, 2021). Moreover, integrating the LNG process with solar-based energy sources is proposed in two studies on open literature. The first utilizes the PV panels to generate power and is limited only to small-scale LNG plants (Afrouzy and Taghavi, 2021). The other one uses an oxy-fuel power cycle to generate power with the use of LNG cold energy as heat sink through the regasification process. As the regasification process needs a higher heating load than the heat rejected from the oxy-fuel cycle, an additional solar parabolic trough collector (SPTC) system is used. Therefore, the LNG flow stream is first heated in precoolers of the oxy-fuel power cycle, then completely evaporated by the thermal energy provided by the SPTC. While these studies are feasible for the LNG at the regasification phase, there is no study about the recovery of the flash-gas from the LNG system at the production phase. Many LNG exporting countries such as the USA, Qatar, Australia, Canada, Algeria, Egypt, Nigeria, and UAE have also great potential for CSP application. Most of these countries have already operational or under-construction CSP projects as shown in Table 1. Thus, integrating LNG plants with the CSP field as proposed in this study will be feasible from a technical and economical point of view. However, the location of the LNG storage should be close enough to the potential location of the CSP field. A large distance between these locations may limit the application of the integrated system unless the connection between them through pipelines is economically feasible. In this case, an economic assessment should be conducted to compare the benefits of flash-gas recovery to the expenditure for the pipeline-based connection.

Table 1
Examples of countries that export LNG with their total operational or under construction CSP projects (Countries with largest liquefied natural gas, 2022; National Renewable Energy Laboratory, 2022; Elbeh and Sleiti, 2021).

Country	LNG export, (million metric tons per year)	Total operational/under construction/under development CSP projects, (MW)
USA	71.6	1740.0
Australia	87.6	152.5
Algeria	29.3	20.0
UAE	7.60	700
Egypt	1.80	20.0

In this work, a novel integration is proposed between the C3MR process and the concentrated solar power system (CSP). The solar energy of the CSP system and the flash-gas from the C3MR are used to drive an intercooled supercritical carbon dioxide (sCO_2) power block. Furthermore, the cold energy of the flash-gas is used in the precooling process of the sCO_2 power cycle. The proposed hybrid system is investigated for five different cases (discussed in Section 5.2) which either eliminate the CO_2 emissions (100% reduction) or reduce the emissions by more than 30%. The selection of the sCO_2 power cycle as the power block for the CSP system instead of the steam Rankine cycle (SRC) is due to several unique features of the sCO_2 power cycles over the SRC. First, the sCO_2 power cycle is more efficient than SRC (typically by 2%–4% at similar operating conditions Reyes-Belmonte et al., 2017; Sleiti et al., 2022). Second, the operation of the sCO_2 power at supercritical pressure tremendously reduces the size of the cycle components compared to that of SRC, which reduces the costs of the turbomachinery components (Wang et al., 2017; Zhu et al., 2017; Syblik et al., 2023). Third, the sCO_2 power cycle is much simpler than SRC and has a potential for very high-temperature operations (750–1200 °C) with energy efficiency between 50%–60% (Wang et al., 2022). Among many power block configurations, the intercooled layout is chosen as it is the best option from the energy point of view (Zhu et al., 2017; Wang et al., 2018). The novelty aspects and contributions of the present work can be summarized as:

- Introducing a novel hybrid integration between the C3MR process and CSP system using an intercooled sCO_2 power block.
- Utilizing the flash-gas and its cold energy to support the sCO_2 power block, which minimizes the CSP field size, and eliminates the need for TES or minimizes their size.
- Developing thorough energetic, exergetic, economic, and environmental analyses to evaluate the performance indicators of the proposed hybrid system compared to conventional gas-turbine-based systems.
- Optimizing the operating parameters of the hybrid system to further enhance its economic and environmental benefits.

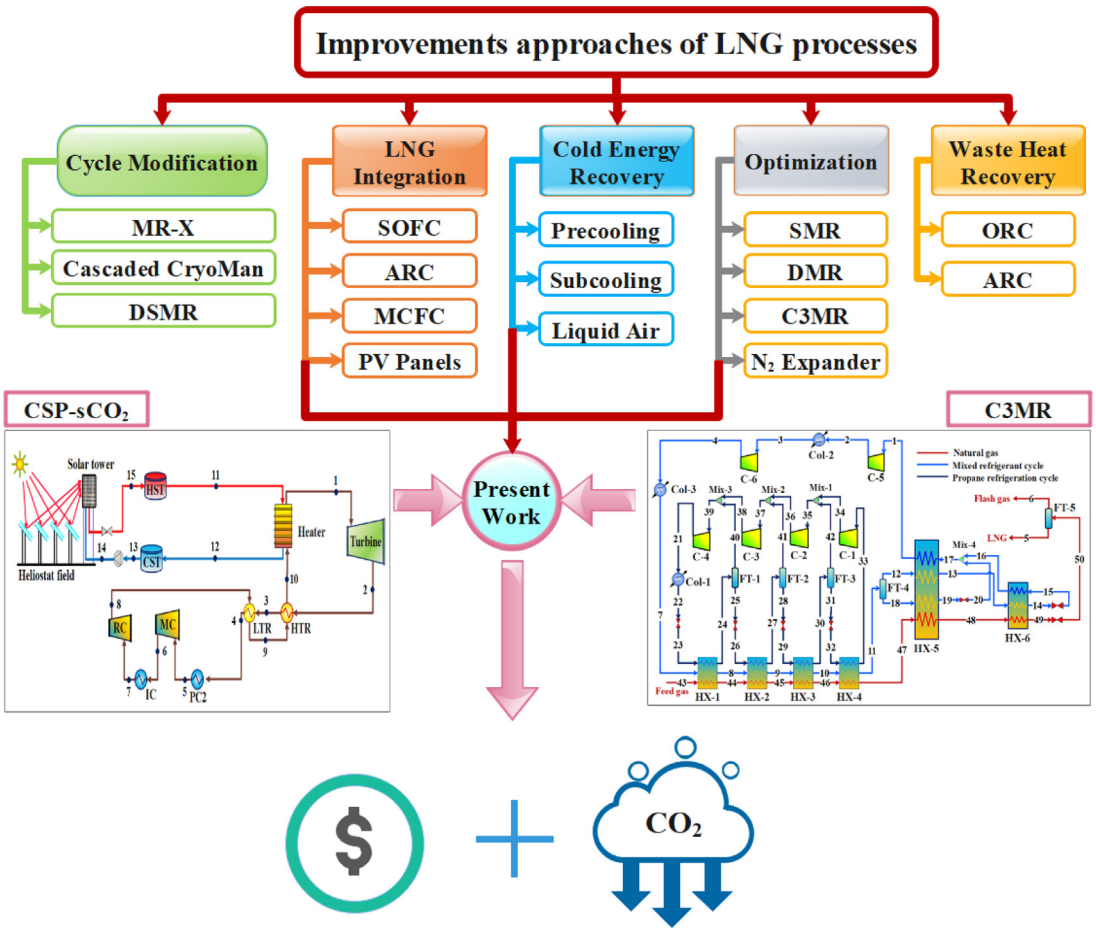

Fig. 1. Improvement approaches of the LNG processes with contributions of the present work.

The rest of the manuscript is organized as follows: Section 2 provides an overview of the configuration and operating mechanism of the proposed hybrid system. In Section 3, we present energetic, exergetic, and economic models of the system, while Section 4 explains simulation procedures and model validation. Section 5 contains a detailed discussion of the study's results. Section 5.1 analyzes the performance of the C3MR process, followed by an examination of the CSP integration cases in Section 5.2. Section 5.3 introduces a comprehensive economic comparison between the investigated cases and other systems/technologies available in the literature. Sections 5.4, 5.5, and 5.6 present sensitivity, optimization, and environmental analyses of the proposed system, respectively. Finally, the major findings are summarized in Section 5. respectively. Finally, the major findings are summarized in Section 5.

2. Description of hybrid CSP-sCO$_2$ power plant and C3MR LNG process

The aforementioned five improvement approaches of the LNG processes are summarized in Fig. 1. The scope of this study covers three enhancement approaches which are LNG integration, cold energy recovery, and optimization. Several benefits could be achieved from integrating the CSP-$_S$CO$_2$ power system with the C3MR process which such as:

(i) The use of the flash-gas to drive an auxiliary heater (as explained in Section 2) could eliminate the need for thermal energy storage for the CSP system. This significantly reduces the capital and operational costs of the CSP system.

(ii) Recovering the cold energy of the flash-gas reduces the cooling load of the sCO$_2$ precooler and intercooler processes which minimizes the operational costs of the sCO$_2$ plant.

(iii) The use of the flash-gas as proposed in (i) and (ii) enhance the economic benefits of the C3MR. This is because recovering the cold energy of the flash-gas and reliquefying it through the C3MR system increase the power consumption and configuration complexity of the process.

(iv) Driving the sCO$_2$ power by the CSP system and the flash-gas of the C3MR eliminates the need for a large-scale oxy-combustor which minimizes the capital cost of the sCO$_2$ plant.

(v) The CO$_2$ emissions could be reduced significantly compared to the conventional oxy-fuel sCO$_2$ power system and C3MR system driven by Brayton gas cycles.

The integration between the CSP-sCO$_2$ power plant with the C3MR LNG process is schematically presented in Fig. 2. The C3MR liquefaction process incorporates two refrigeration cycles, first, the three-stage propane pre-cooling cycle (referred to as C3 Pre-cooling in Fig. 2), and the other one is the mixed-refrigerant cycle (referred to as MR loop in Fig. 2). The pre-treated NG (NG) enters the C3 precooling cycle mostly at a pressure of 65 bar and temperature higher than 25 °C (state a) and flows through the pre-cooling heat exchangers (C3MR detailed flowsheet is presented in Fig. 3) to be cooled down to −33 °C or −35 °C (state c). Then, it passes through the main cryogenic heat exchanger (MCHE) where it is further cooled to a temperature between −155 °C to −160 °C (state d). Then, it is throttled to

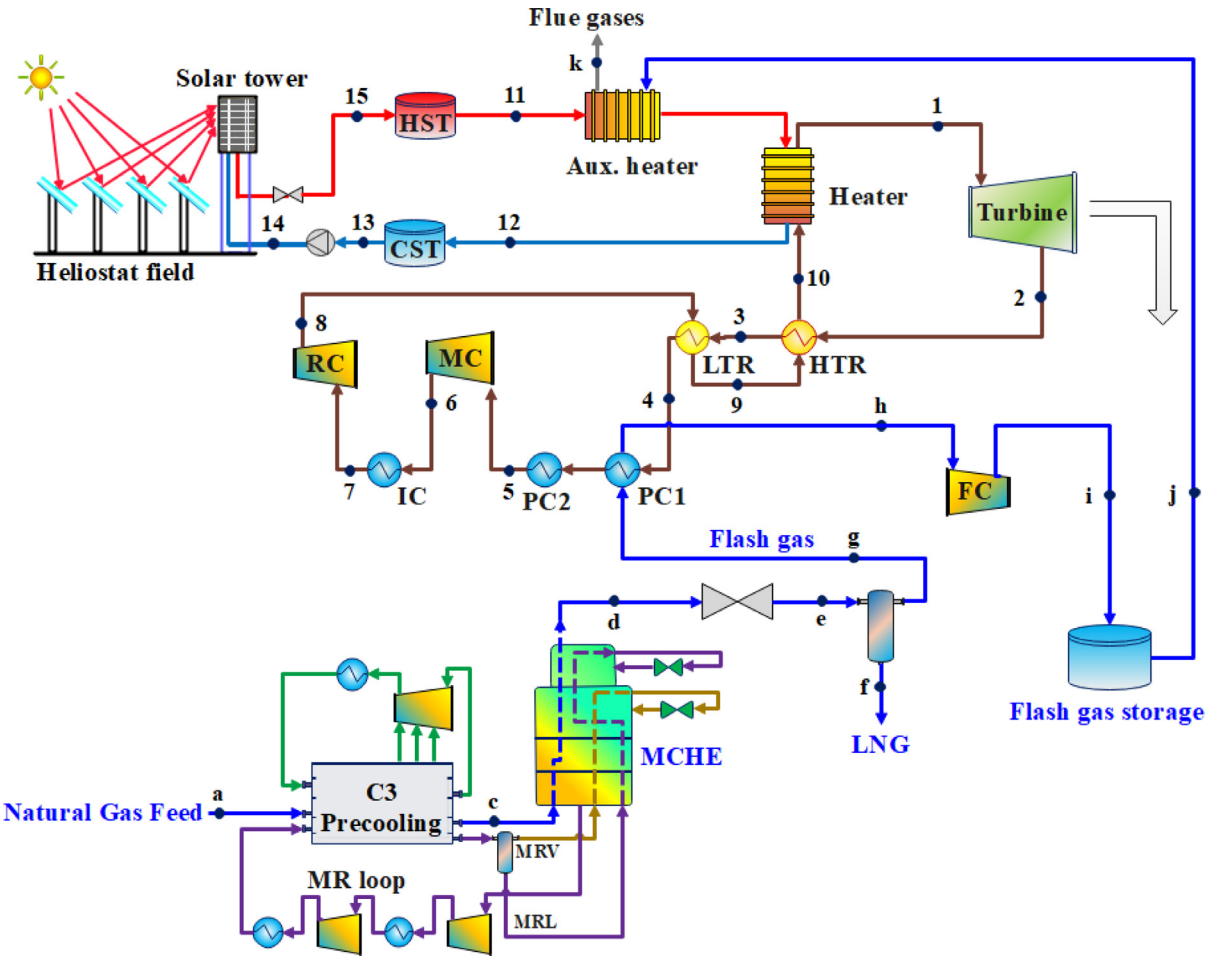

Fig. 2. Layout of the hybrid CSP-sCO2 power plant and C3MR LNG process.

near ambient pressure and temperature of −162 °C (state e) where it is liquefied. During the throttling process, part of the NG flow is evaporated as flash-gas (state g), which is used (in a conventional system) as fuel for the gas turbine after being warmed and compressed to suitable conditions.

In the present hybrid system, the power demand for the C3MR LNG process will be supplied by the CSP-sCO$_2$ power plant aided by an auxiliary heater using the flash-gas produced from the C3MR process. The CSP field equipped with TES can be designed to match the demand power of the power cycle for the full operational time (24 h/day). This design eliminates the CO$_2$ emissions associated with conventional gas turbines. However, the capital investment is large and the LCOE remains at a high level (>14¢/kWh), which is not competitive with gas or combined power cycles. However, considering the relatively large flash-gas flow, an auxiliary heater can be integrated with the CSP to reduce its field size, reduce the capacity of TES, or eliminate the need for the TES. This significantly minimizes the capital cost of the CSP system and mitigates the CO$_2$ emissions as well. It is worth mentioning that splitting the HTR and LTR is usually done if the flow rate through them is different. However, even with the same flow rate, utilizing a single recuperator to recover a large amount of heat is not practical, as it requires a huge size. Therefore, the recuperator is split into HTR and LTR in this study to maintain a reasonable size. Such a split in the sCO$_2$ power block is employed in several studies (Luo and Huang, 2020; Utamura et al., 2016; Sleiti and Al-Ammari, 2021).

The operation of the hybrid CSP-sCO$_2$ plant and C3MR LNG process can be explained as follows: During sunshine hours, the thermal energy demand of the sCO$_2$ cycle is provided directly by the hot molten salt leaving the receiver (state 15) and the excess energy is stored in the hot storage tank (HST). As the receiver energy drops below the demand thermal energy, the stored energy in the HST is used for the designed capacity (for example 10 h.). During the night-time, the AH generates the required thermal power by combusting the flash-gas delivered from the storage (state j) at a controlled flow rate. To make this feasible, the very cold flash-gas (−126 °C) first warmed (process g–h) by absorbing part of the heat rejected in the precooling process of the hot-side sCO$_2$ flow (4–5). Then, the flash-gas is compressed (h–i) and stored in the flash-gas storage. Utilizing the cold energy of the flash-gas in the precooling process (through PC1) minimizes the water consumption (for wet-cooling) or the power consumption (for dry-cooling). Based on the integration scenario, the flash-gas can be used to partially aid the TES or eliminate the need for it as discussed in Section 5.2. Therefore, if the amount of the flash-gas exceeds that required for the auxiliary heater, the excess amount can be recycled to the feed line. The recycled flash-gas reduces the amount of subcooling required in the MCHE and shifts the power from the MR loop to the flash-gas compressor (FC). Thus, either the flash-gas is recycled or exported to the auxiliary heater; the power demand will be the same as that for gas turbines.

3. Mathematical modeling

3.1. C3MR LNG process model

Fig. 3 presents the detailed flowsheet of the simulated C3MR process in this study. The C3MR simulations are performed using

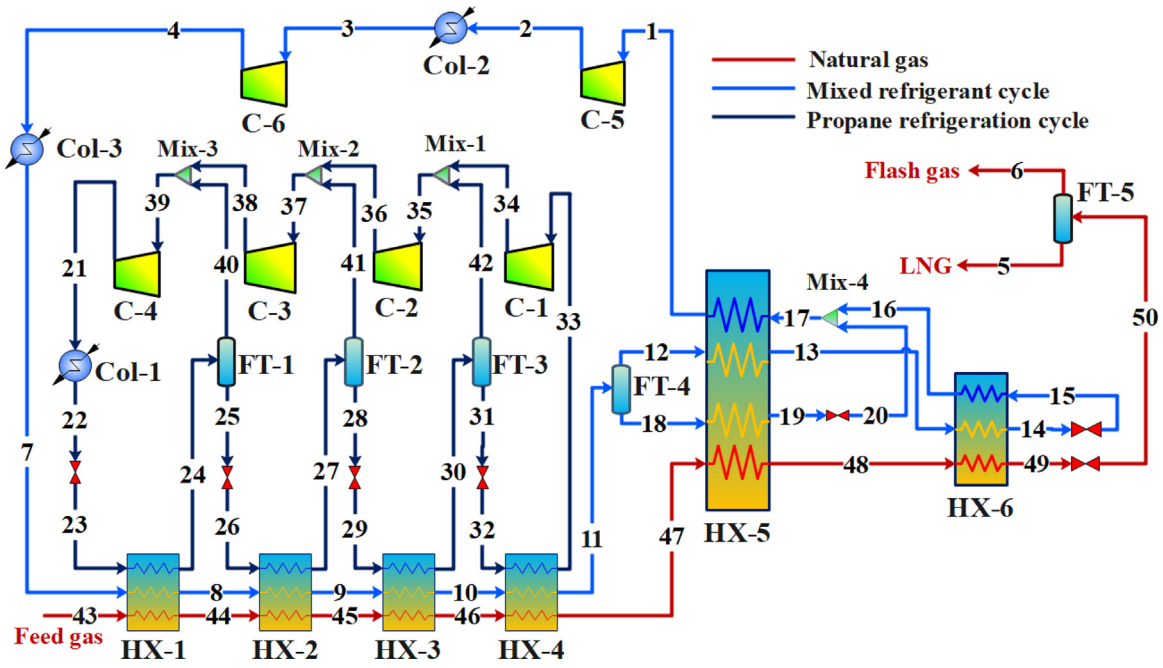

Fig. 3. Layout of the C3MR LNG process.

Aspen HYSYS. Peng–Robinson equation of state is implemented because of its accurate calculation performance and applicability in a wide range of temperatures and pressures in defining the properties of light hydrocarbon mixtures. Furthermore, the C3MR process is modeled using the following assumptions:

- For C3MR compressors, the isentropic efficiency is assumed 75% and the mechanical efficiency is 90%.
- Phase separators and mixers are assumed to operate without pressure drops.
- The design NG flow is assumed to be supplied at 130 kg/s.
- The NG is assumed to be already pre-treated.

The performance of the C3MR process is expressed in term of its coefficient of performance (COP) as a cryogenic refrigeration process, which is defined as (Sleiti and Al-ammari, 2022):

$$COP = \frac{\sum_{i=1}^{i=6} Q_{HX,i}}{\sum_{j=1}^{j=6} \dot{W}_{HX,j}} \tag{1}$$

where $\sum_{i=1}^{i=6} Q_{HX,i}$ is the total cooling load of the C3MR heat multi-stream heat exchangers, which can be expressed as:

$$\sum_{i=1}^{i=6} Q_{HX,i} = Q_{HX,1} + Q_{HX,2} + Q_{HX,3} + Q_{HX,4} + Q_{HX,5} + Q_{HX,6} \tag{2}$$

And $\sum_{j=1}^{j=6} \dot{W}_{HX,j}$ is the total compression power of the C3MR compressors, which can be expressed as:

$$\sum_{j=1}^{j=6} \dot{W}_{HX,j} = \dot{W}_{HX,1} + \dot{W}_{HX,2} + \dot{W}_{HX,3} + \dot{W}_{HX,4} + \dot{W}_{HX,5} + \dot{W}_{HX,6} \tag{3}$$

3.2. CSP model

In this section, an integrated model is developed for the heliostat field, solar receiver, thermal storage subsystem, and auxiliary heater. Referring to Fig. 2, the total heat absorbed by the receiver ($Q_{rec,in}$) is given as (Yang et al., 2020):

$$Q_{rec,in} = DNI \cdot A_{hel} \cdot \eta_{hel} \cdot \alpha_{rec} \tag{4}$$

where DNI, A_{hel}, η_{hel}, and α_{rec} are the direct normal irradiance, the total area of the heliostat field, the heliostat field efficiency, and the absorptivity of the receiver, respectively. Part of the absorbed heat by the receiver is delivered to the molten salt ($Q_{rec,out}$) and the other part is lost to the ambient by radiation ($Q_{rec,rad}$) and convection ($Q_{rec,conv}$) such that:

$$Q_{rec,in} = Q_{rec,out} + Q_{rec,rad} + Q_{rec,conv} \tag{5}$$

Let $T_{rec,o}$ and $T_{rec,i}$ to be the outer and inner wall temperatures of the receiver tube, respectively. The heat losses by radiation and convection are defined as (Sleiti and Al-ammari, 2021):

$$Q_{rec,rad} = \sigma \cdot \varepsilon_{rec} \cdot A_{rec}((T_{rec,o} + 273)^4 - (T_{sky} + 273)^4) \tag{6}$$

where T_{sky} is the sky temperature, which is given as (Sleiti and Al-ammari, 2021):

$$T_{sky} = 0.0552 \times (T_o)^{1.5} \tag{7}$$

$$Q_{rec,conv} = h_{rec,conv} \cdot A_{rec}(T_{rec,o} - T_o) \tag{8}$$

where $h_{rec,conv}$ is the convective heat transfer coefficient between the receiver and ambient air, (Sleiti and Al-ammari, 2021):

$$h_{rec,conv} = 5 + 3 \cdot V_{wind} \tag{9}$$

Then, the heat transferred to the inner wall by conduction is calculated as:

$$Q_{rec,out} = \frac{2\pi \cdot k_{tube} \cdot l_{tube}(T_{rec,o} - T_{rec,i}) \cdot N_{tube}}{\ln\left(d_{o,tube}/d_{i,tube}\right)} \tag{10}$$

Then, the heat is transferred to the molten salt by convection; thus, it is expressed in terms of the inner receiver temperature and the average temperature of the molten salt ($T_{avg,salt}$) such that (Wang and He, 2017):

$$Q_{rec,out} = h_{salt} \cdot (\pi \cdot D_{i,tube} \cdot l_{tube}) \cdot (T_{rec,i} - T_{avg,salt}) \cdot N_{tube} \tag{11}$$

In terms of the mass flow rate and enthalpies of the molten salt at the inlet and outlet of the receiver, $Q_{rec,out}$ is defined as (based on the state points in Fig. 2):

$$Q_{rec,out} = \dot{m}_{salt,rec} \cdot (h_{15} - h_{14}) \tag{12}$$

The efficiency of the solar field is:

$$\eta_{I,CSP} = Q_{rec,out}/(DNI \cdot A_{hel}) \tag{13}$$

The salt storage tanks are assumed to be insulated and the thermal loss is ignored. The amount of the thermal energy charged or discharged from the HTS as well as the energy that needs to be generated by the auxiliary heater (AH) depends on the time during the day. Therefore, during sunshine hours:

$$If\ Q_{rec,out} > Q_{heater} \rightarrow Q_{st,i} = Q_{rec,out} - Q_{heater};\ Q_{AH} = 0 \tag{14}$$

$$If\ Q_{rec,out} < Q_{heater}\ \&\ Q_{rec,out} > 0 \rightarrow Q_{st,o}^{sunshine} = Q_{heater} - Q_{rec,out};\ Q_{AH} = 0 \tag{15}$$

After sundown, $Q_{rec,out} = 0$, and the remaining energy in the hot storage tank ($E_{HST}^{sundown}$) is:

$$E_{HST}^{sundown}(\text{kWh}) = \Big[\sum \big(Q_{st,i} \times charge\_time\big) - \big(Q_{st,i} \times dicharge\_time\big)\Big]_{sunshine} \tag{16}$$

This energy is exported to the heater at the demand rate (Q_{heater}), thus, $E_{HST}^{sundown}$ will drive the heater for some hours:

$$discharge\_time_{night} = E_{HST}^{sundown}/(Q_{heater}) \tag{17}$$

Once the thermal energy in the hot-salt tank (HST) is exploited (or does not match the demand during the last discharge hour), AH will work to generate the thermal power required to drive the heater. Therefore,

$$if\ Q_{st,o}^{night} < Q_{heater}\ but\ Q_{st,o}^{night} > 0 \rightarrow Q_{AH} = Q_{heater} - Q_{st,o}^{night} \tag{18}$$

$$if\ Q_{st,o}^{night} = 0 \rightarrow Q_{AH} = Q_{heater} \tag{19}$$

During the operation time of the AH, the mass flow rate of the flash-gas is:

$$Q_{AH} = \dot{m}_{fg,AH} \times LHV_{fg} \tag{20}$$

3.3. sCO_2 power cycle model

The energetic model of the sCO_2 power cycle is developed based on the application of the mass and energy balance principles on each component (Sleiti et al., 2021a):

$$\sum \dot{m}_i = \sum \dot{m}_o \tag{21}$$

$$\sum \dot{Q} + \sum \dot{m}_i h_i = \sum \dot{W} + \sum \dot{m}_o h_o \tag{22}$$

Moreover, the exergy analysis is implemented by the exergy balance principle such that (Sleiti and Al-Ammari, 2021):

$$\dot{E}_Q + \sum \dot{E}_i = \dot{E}_W + \sum \dot{E}_o + \dot{E}_D \tag{23}$$

The exergy at each state is defined as:

$$\dot{E} = \dot{E}_{ph} + \dot{E}_{ch} \tag{24}$$

where $\dot{E}_{ph}$, and $\dot{E}_{ch}$ are the physical and chemical exergies of each state. The physical exergy is defined as:

$$\dot{E}_{ph} = \dot{m}\varphi \tag{25}$$

$$\varphi = (h - h_o) - T_o(s - s_o) \tag{26}$$

where h_o, T_o, and s_o are the enthalpy, temperature, and entropy at the dead state of the exergy analysis (taken as $T_o = 37\ ^\circ\text{C}$, $P_o = 1$ bar). The net output power of the CSP-sCO_2 system is (assuming a one-shaft-arrangement):

$$P_{net} = \eta_{g,c}(\dot{W}_t - \dot{W}_{MC} - \dot{W}_{RC}) - \eta_{g,p}\dot{W}_{pump} \tag{27}$$

The energy efficiency of the sCO_2 cycle is:

$$\eta_{I,sCO_2} = P_{net}/Q_{heater} \tag{28}$$

And the exergy efficiency is:

$$\eta_{II,sCO_2} = \frac{\sum \dot{E}_{P,k}}{\sum \dot{E}_{F,k}} \tag{29}$$

The detailed energetic and exergetic models of each component are given in Supplementary material B (Table SB.2). It should be noted that due to the dramatic change of the sCO_2 specific heat through the cold side of the LTR and HTR, their calculations were implemented using the discretized model developed by Sleiti et al. (2021a).

The economic model of the CSP-sCO_2 model is developed by estimating the capital costs of each component using the correlations presented in Supplementary material B (Table SB.5). The construction cost is assumed to be 12% of the component capital cost. Furthermore, the operating and maintenance costs are set as 8% of the capital cost of the system. The LCOE and the calculations of the present values are conducted as defined in (Sleiti et al., 2021b; Wright et al., 2017).

$$LCOE = \frac{PC - PV_{DTS} + PV_{LOC} - PV_{SC}}{LEP} \tag{30}$$

$$PC = \sum (Component\ cost + Installation\ cost)_k \tag{31}$$

$$PV_{DTS} = TR \times PC/(1 + DR)^{DP} \tag{32}$$

$$PV_{LOC} = n * (OMC + Cost\ of\ the\ fuel)\ /(1 + DR)^n \tag{33}$$

$$LEP = PUF \times n \times P_{net} \times 8760 \tag{34}$$

where PC, TR, DR, DP, n, PUF, and LEP are the total project cost, tax rate, discount rate, depreciation period, project lifetime, plant utilization factor, and plant life energy production, respectively. For more conservative analysis, the salvage present value is assumed zero.

4. Simulation procedures and validation

This section describes the simulation and validation of the C3MR model in Section 4.1, and of the CSP-sCO_2 model in Section 4.2.

4.1. Simulation procedures and validation of the C3MR model

Before the simulation of the C3MR at the design NG flow, the Aspen HYSYS results were first validated against the results from Ghorbani et al. (2016) at identical composition for Composition 1 in Table 2 (for both the NG and MR). The validation results are summarized in Supplementary material B (Table SB.1), where the relative errors are almost negligible (less than 0.40%) indicating accurate validation.

After the validation process, the C3MR process is simulated under the desired NG flow rate (130 kg/s) and the temperatures of the heat exchanger streams are varied to improve and optimize the quality of their design. The composite curves of the heat exchangers (HX-1 to HX-6 of Fig. 3) and the overall composite curve (OCC) are shown in Fig. 4. Note that the propane flow at the exit of HX4 is in superheated phase (Fig. 4(d)) to ensure that no liquid drops at the inlet of the first compressor (C-1). Based on the OCC (Fig. 4(g)), it can be noted that the difference between the refrigerant curve (cold composite) and the NG curve (hot composite) is sufficiently minimized. However, further improvement on the heat exchanger performance could be enhanced by optimizing the mixed-refrigerant of the MR refrigeration process.

4.2. Simulation procedures and validation of the CSP-sCO_2 power cycle models

The operating parameters of the CSP-sCO_2 system are presented in Table 2. The design net power capacity of the integrated

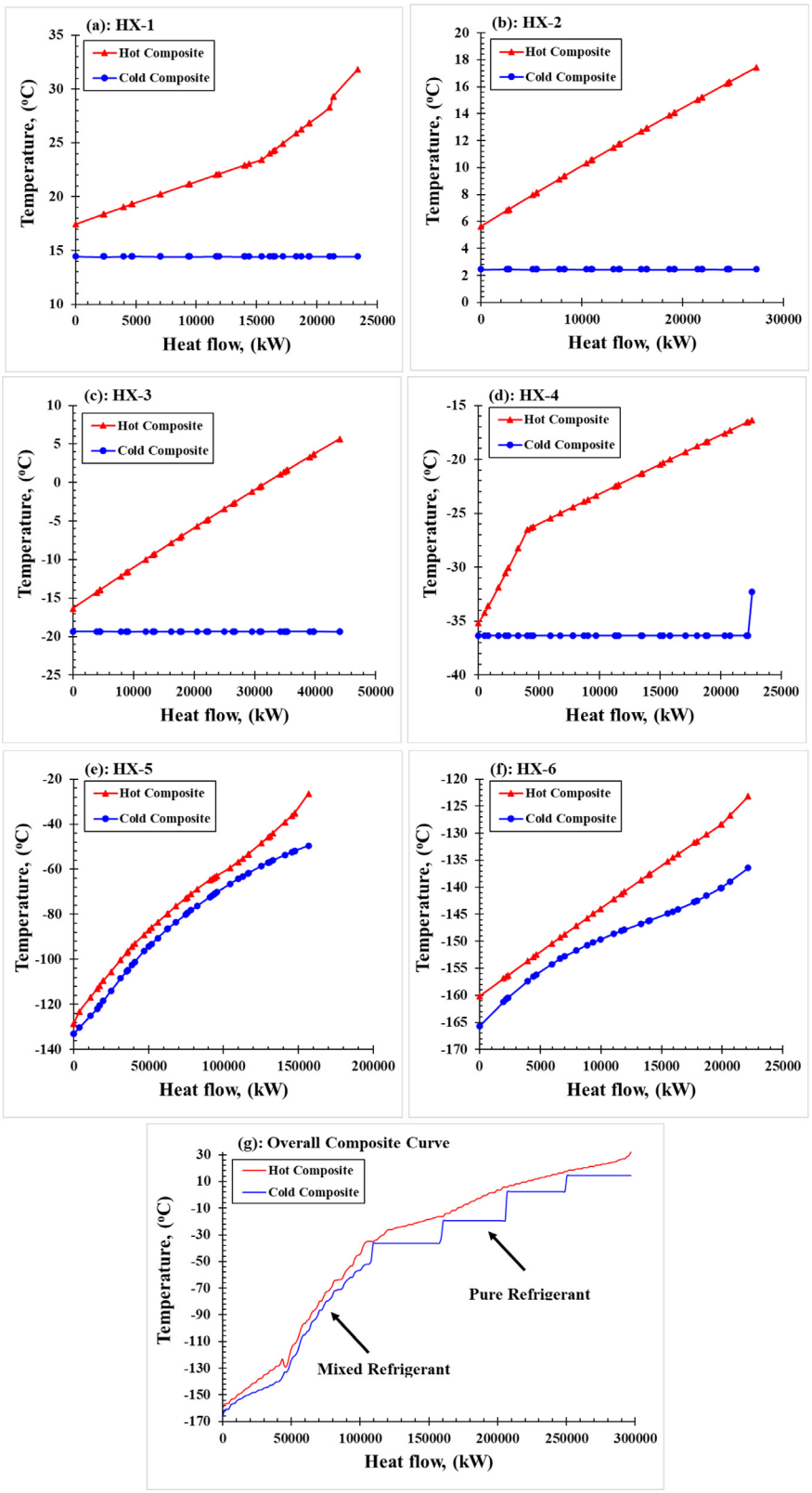

Fig. 4. Composite curve of the heat exchangers (a–f) and the overall composite curve of the process (g).

system was set as 135 MW. Real-field CSP systems are already available for such capacity and the sCO_2 power cycles are currently developing for large power production with a range from 50 MW to higher than 300 MW (Scaccabarozzi et al., 2017; Rogalev et al., 2019). As shown in Fig. 5, the solution procedures start by determining the composition of the feed NG and mixed-refrigerant of the C3MR process and their inlet conditions to HX-1. Then, in Aspen Plus, the temperatures of hot streams

Table 2
Input parameters of the direct oxy-fuel preheated sCO_2 cycle.

	Parameter	Range/Design value
CSP field	Receiver absorptivity, α_{rec}	0.94 (Yang et al., 2020)
	Heliostat width, (m)	12 (Sleiti and Al-Ammaria, 2022)
	Heliostat height, (m)	12 (Sleiti and Al-Ammaria, 2022)
	Number of heliostats	5500–15 900
	Tube outer diameter, $d_{o,tube}$ (mm)	42 (Yang et al., 2020)
	Tube inner diameter, $d_{i,tube}$ (mm)	40.35 (Yang et al., 2020)
	Number of panels	20 (Sleiti and Al-Ammaria, 2022)
	Tower height, H_{tower} (m)	195
	Receiver height, $H_{receiver}$ (m)	21 (Sleiti and Al-Ammaria, 2022)
	Receiver diameter, $D_{receiver}$ (m)	15 (Yang et al., 2020)
Cycle parameters	Higher pressure, P_{max} (bar)	200–300 (Sleiti et al., 2021a)
	Lower pressure, P_{min} (bar)	75–85 (Sleiti et al., 2021a)
	Maximum cycle temperature, T_{max} (°C)	550–750 (Sleiti et al., 2021a)
	Compressor inlet temperature, T_{min} (°C)	32 (Wet), 50 (Dry)
	Net electrical power, P_{net} (MW)	135
	Efficiency of the generator, $\eta_{g,c} = \eta_{g,p}$, (%)	98 (Yang et al., 2020)
	Efficiency of the gas turbine, η_{GT} (%)	93 (Yang et al., 2020)
	Efficiency of the gas compressors, η_{GC} (%)	89 (Yang et al., 2020)
	LHV_{fg} (kJ/kg)	45 000 (Sleiti et al., 2022)
Pressure drops	Heater and Auxiliary heater	3 (Zhang et al., 2010)
	Recuperators (high-pressure side) (%)	1 (Scaccabarozzi et al., 2016)
	Recuperators (low-pressure side) (%)	3 (Zhang et al., 2010)
	Precoolers and intercooler	2 (Scaccabarozzi et al., 2016)
Economic parameters	Plant lifetime (years)	20 (Sleiti et al., 2021b)
	Depreciation period (DP) (years)	10 (Sleiti et al., 2021b)
	Tax rate (%)	35 (Sleiti et al., 2021b)
	Plant utilization factor (*PUF*) (%)	68 (Sleiti et al., 2021b)
	Cost of the fuel ($/kWh$_e$)	0.07 (Sleiti et al., 2021b)
	Operating and maintenance cost, (%) from capital cost	8 (Sleiti et al., 2021b)

through HX-1 to HX-6 were set to achieve an optimal cold composite curve compared to the hot composite curve. Then, the power demand, LNG flow, and flash-gas flow were calculated and exported to the model of the CSP-sCO_2 system. The latter is modeled by creating energetic, exergetic, and economic models in Engineering Equation Solver (EES). By defining the operating parameters of the CSP field and sCO_2 power cycle, the performance indicators (η_{I,sCO_2}, $\eta_{I,CSP}$, η_{II,sCO_2}, *and LCOE*) are calculated. After that, based on the sensitivity analysis, the operating parameters of both C3MR and CSP-sCO_2 systems are optimized in Aspen Plus and EES using a genetic algorithm (GA) approach. However, the GA approach may fall into a local optimum and to get out of this local optimum, the results can be tested at a higher mutation rate. The higher the mutation rate is, the more range will be searched and the higher the chance that the global optimum is found. The obtained results are compared and discussed for different cases as explained in Section 5.2.

For the validation purposes of the CSP-sCO_2 integrated model, the generated code in EES is adequately modified to match the layout of the precompression CSP-sCO_2 power cycle investigated by Ma et al. (2020). In their system, there is no integration between the C3MR process and the CSP-sCO_2 power system; therefore, there is no flash-gas to be used in the precooling process and the thermal power generation for the heater of the power block. The comparison was implemented at the same net output power (100 MW), DNI (719 WS/m^2), and T_{max} of 550 °C at wet and dry-cooling conditions. The major reported output results are compared as shown in Supplementary material B (Table SB.6). In general, the results show very good agreement with an average error of 1.24% in the energy efficiency and the LCOE of the system. The number of subsections used in the models of the LTR and HTR as well as the calculation methodology of the overall heat transfer coefficient were not reported in Ma et al. (2020). Therefore, the models of the HTR and LTR used in Ma et al. (2020) compared to the finer discretized models used in the present study cannot be matched by using the same effectiveness only (as the specific heat of the CO_2 dramatically changes on the high-pressure side). Thus, a reasonable average error of 3.41% is noted for the sCO_2 temperature at the inlet of the heater.

5. Results and discussion

This section is dedicated to a thorough examination of the study's findings. Section 5.1 provides an analysis of the performance of the C3MR process, followed by an examination of the CSP integration cases in Section 5.2. Section 5.3 offers a comprehensive economic comparison between the investigated cases and other systems/technologies available in the literature. In Sections 5.4, 5.5, and 5.6, the proposed system is subject to sensitivity, optimization, and environmental analyses, respectively.

5.1. C3MR LNG process analysis

For the analysis of the C3MR process at medium to large-scale LNG production, the energetic simulation for the LNG production and power consumption is performed within feed gas flow (NG) between 50 kg/s to 150 kg/s. Also, the results are presented for two different sets of the compositions of the feed gas to the C3MR and its mixed refrigerant, which are referred to as Composition 1 and Composition 2 (shown in Table 3). The detailed state points of the C3MR process for composition 1 at feed gas flow of 130 kg/s are presented in Supplementary material A (Table SA.1). It is found that the average percent of the produced LNG is 92.20% (composition 1) and 97.82% (composition 2) from the feed gas flow. This yields a plant capacity from 1.45MTPA to 4.63MTPA, which covers the scale of the existing C3MR plants. As shown in Fig. 6, the flash-gas flow for composition 2 is lower than that of composition 1 by 72%, and the compression power for composition 2 is higher than for composition 1 by 15%. In addition, the cooling duty of the C3MR heat exchanger for composition 1 is higher than that of composition 2 by 12%, which improves its COP by 27% over that of composition 2. Therefore, the analysis of the integrated C3MR-CSP system is based on the results of composition 1. Moreover, the nominal power demand of 135 MW

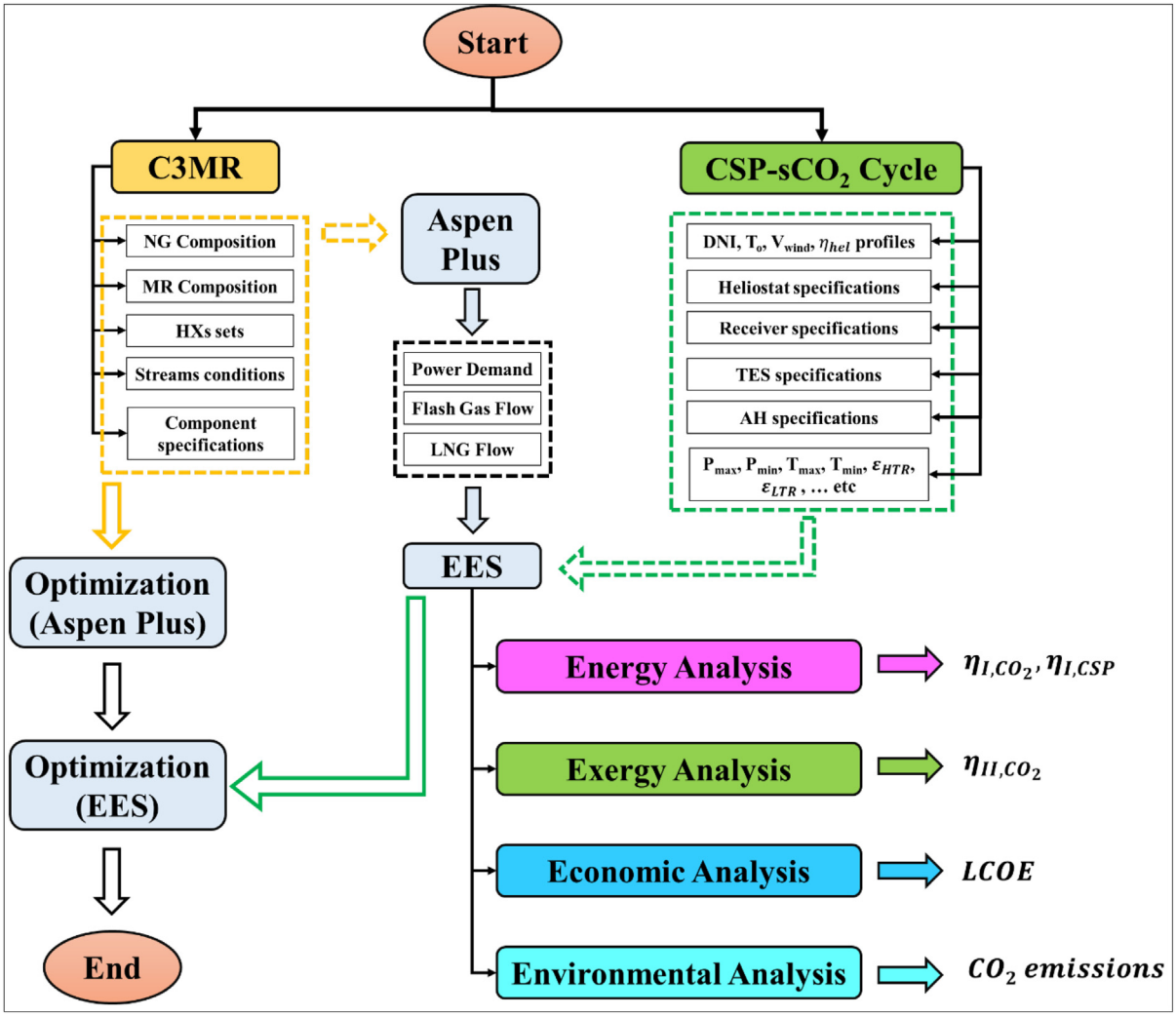

Fig. 5. Flow chart of the solution procedures.

Table 3
Details of the two considered compositions for the C3MR feed NG (NG) and mixed-refrigerant (MR) (Primabudi et al., 2019; Ghorbani et al., 2016) cas.

Component	Composition 1		Composition 2	
	NG	MR	NG	MR
Nitrogen	0.0401	0.0700	0.0010	0.1000
Methane	0.8748	0.4181	0.8600	0.6000
Ethane	0.0550	0.2989	0.0750	0.2000
Propane	0.0212	0.2130	0.0640	0.1000
Butane	0.0089	0.0000	0.0000	0.0000

corresponds to a feed gas flow of 130 kg/s, LNG flow of 119.9 kg/s, and flash-gas flow of 10.1 kg/s.

About 8% to 12% of the feed gas to the liquefaction plant is consumed to run the process (Mokhatab et al., 2014), which forms a major source of CO_2 emissions. Therefore, replacing these turbines with more efficient power cycles such as the sCO_2 power cycle driven by concentrated solar power tower (to match the large power demand) will offer more commercial and environmental benefits to the LNG industry. The next section discusses different cases for integration between the C3MR process and CSP-sCO_2 power system and compares the economic results with the existing power technologies.

5.2. CSP integration analysis

Five cases for integration between the C3MR and CSP-sCO_2 power system are introduced. Case-1: C3MR is driven by the CSP system and its TES without using an auxiliary heater (Case-1 abbreviated as (CSP+TES)), see Fig. 7. Case-2: C3MR is driven by the CSP system and its TES with a partial contribution for the auxiliary heater (CSP+TES+AH). Case-3: similar to Case-2 with a mostly equal contribution for the TES and AH. Case-4: similar to Case-2 with a partial contribution for the TES. Case-5: C3MR is driven by the CSP system and AH without TES. In all cases, the cold energy of the flash-gas from the C3MR process is used for partially cooling the sCO_2 flow stream leaving the LTR of the sCO_2 power cycle. Furthermore, in cases 2–5, the auxiliary heater is powered by the flash-gas of the C3MR process.

To investigate the considered cases, real ambient conditions for DNI, ambient temperature, and wind speed for a typical day in Qatar (7 Sept. 2016) are used as presented in Fig. 8. These data depict the general real ambient conditions of those LNG exporting countries with existing or planned CSP projects as mention in Section 2. It can be noted that the maximum DNI occurs near 12:00 PM and the sunshine duration is 12 h with 10 h having a DNI higher than 200 W/m^2. The corresponding heliostat field efficiency was also calculated and presented in Fig. 8. It reaches a maximum value of 67% at 12:00 AM. At these conditions, the solar

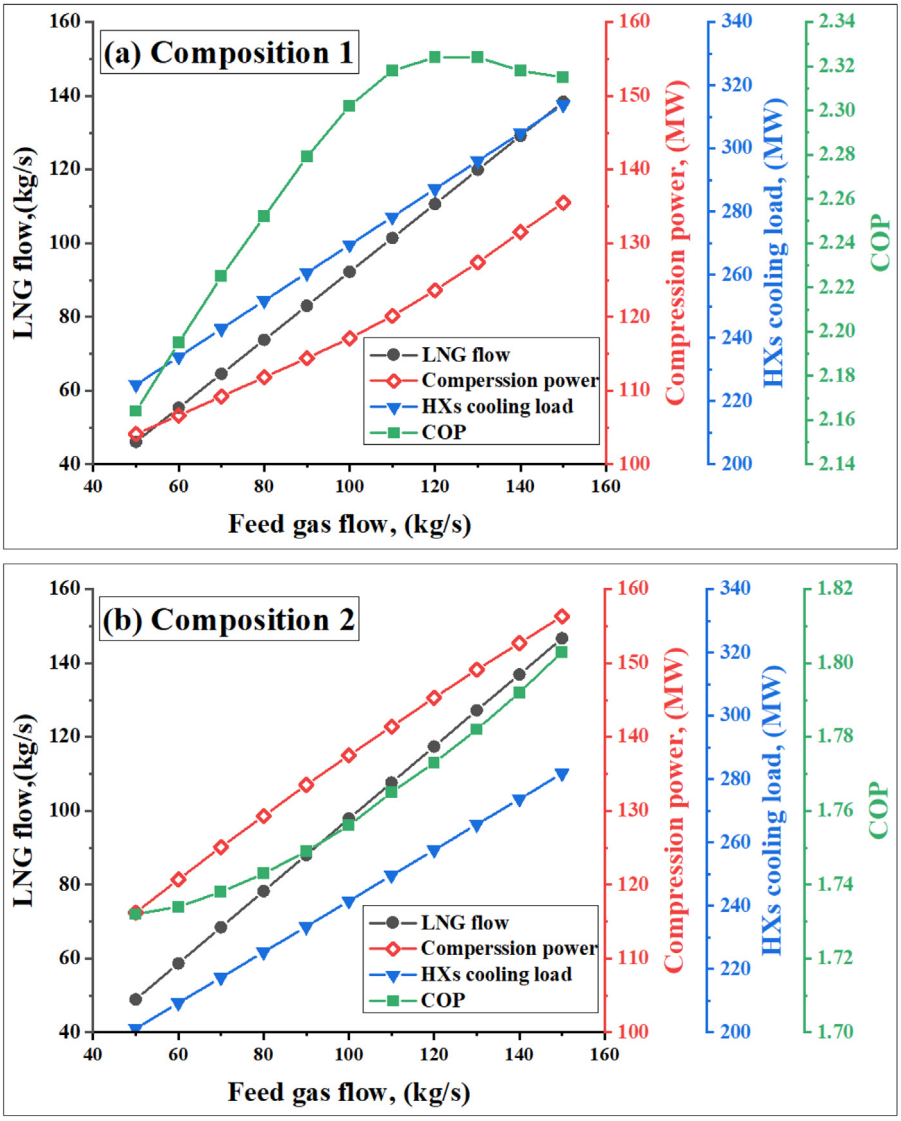

Fig. 6. Performance indicators of C3MR LNG process for (a) composition 1, and (b) composition 2.

Table 4
Comparison between the proposed cases for the integration between the C3MR LNG process and the CSP sCO_2 power system (Wet-cooling).

Case#	Configuration	TES (h)	AH (h)	$N_{heliostat}$	$\eta_{I,CSP}$ (%)	LCOE (¢/kWh)
1	CSP+TES	14	0	15 900	38.45	13.37
2	CSP+TES+AH	11	4	13 000	38.75	10.43
3	CSP+TES+AH	8	9	10 500	38.91	10.02
4	CSP+TES+AH	6	10	9000	38.95	9.85
5	CSP+AH	0	20	5500	38.105	9.39

field of the CSP is sized and analyzed energetically and economically for each case to match the constant power demand of the C3MR process (135 MWe, equivalent to 334 MW_{th}). The variation of the ambient temperature and wind speed during sunshine hours significantly affects the amount of useful energy absorbed by the receiver. Higher ambient temperatures will compensate for the convective energy losses associated with the increase in wind speed. Thus, the profile of the absorbed heat by the receiver ($Q_{rec,out}$) will follow the variation of the DNI rather than the ambient temperature and wind speed as shown in Fig. 9.

Fig. 9 shows the thermal power transfer mechanisms from the receiver and AH to the heater of the sCO_2 cycle and to or out from the TES. Note that Q_{heater} denotes the constant thermal power demand of the sCO_2 cycle heater. $Q_{rec,out}$ refers to the thermal power absorbed by the molten salt through its pass through the receiver. Part of $Q_{rec,out}$ is used to drive the heater and the other part is stored in the hot TES ($Q_{TES,i}$) during the sunshine hours. The amount of $Q_{rec,out}$ and $Q_{TES,i}$ are proportional to the field size of the CSP. To optimize the utilization of the flash gas, the size of the CSP field ($N_{heliostat}$) is reduced to allow more time for the AH contribution. Therefore, as the field size is reduced, the storage capacity is reduced too and the contribution of the AH increases. In addition, the period of operation of the TES and the AH is calculated based on the real-time of sunshine hours and the rate of energy required to drive the power block (using Eqs. (14) to (17)).

The major energetic and economic results of each case are presented in Table 4. The CSP field size is changed to match the desired operating period of the TES. Changing the size of the CSP field (number of heliostats) will change the amount of heat absorbed by the receiver and those lost to the ambient by convection and radiation. Thus, the average thermal efficiency will be changed from one case to another as shown in Table 4. Case-5 (CSP+AH) reduces the heliostat number to 5500 compared to 15900 required for Case-1 (CSP+TES). Although there are CO_2

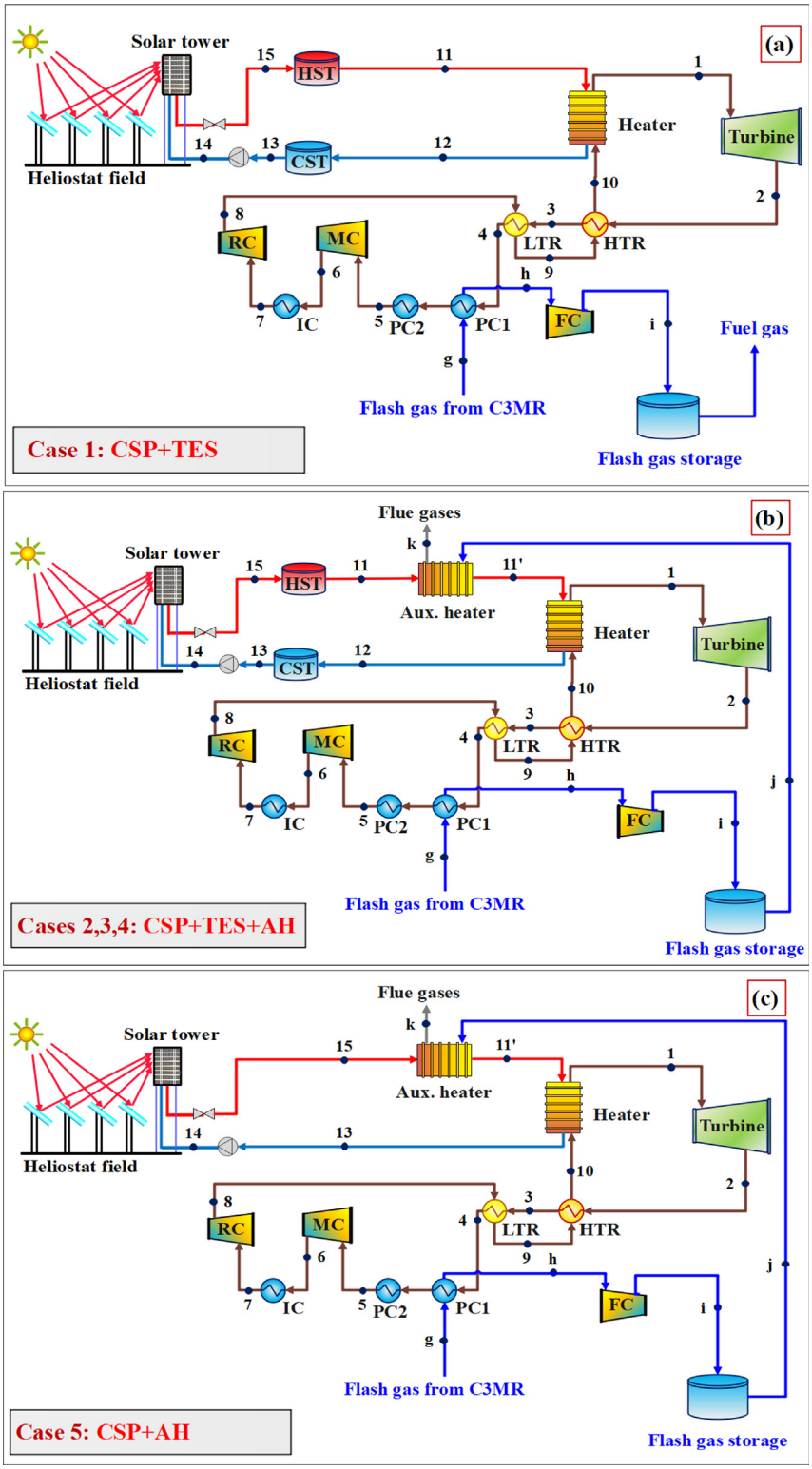

Fig. 7. Schematic diagrams for the integration cases between the C3MR and CSP systems; (a) Case-1: CSP+TES; (b) Cases 2, 3, and 4: CSP+TES+AH; (d) Case-5: CSP+AH.

emissions in Case-5, it is still lower than conventional steam and gas turbines (100% fuel) as the CSP field (without TES) contributes to the energy demand (2.89E+07 MJ/day) by 36% (1.04E+07 MJ/day). As the cost of energy coming from the AH is cheaper than that coming from the CSP, the economic performance of the proposed cases is improved as the share of the AH increases. Thus, Case-5 reduces the LCOE to 9.39 ¢/kWh compared to 13.37 ¢/kWh for Case-1 (30% reduction). As shown in Fig. 9(e), the AH will provide the full energy demand for 13 h/day and partially assist the CSP filed for 7 h/day and being in off-mode for 4 h/day. During the full energy demand hours, the compressed flash-gas is provided to the AH at a flow rate of 8.3 kg/s. In conclusion, Case-5 has the features of the smallest CSP field size, and no TES is used, which significantly reduces the capital investment costs

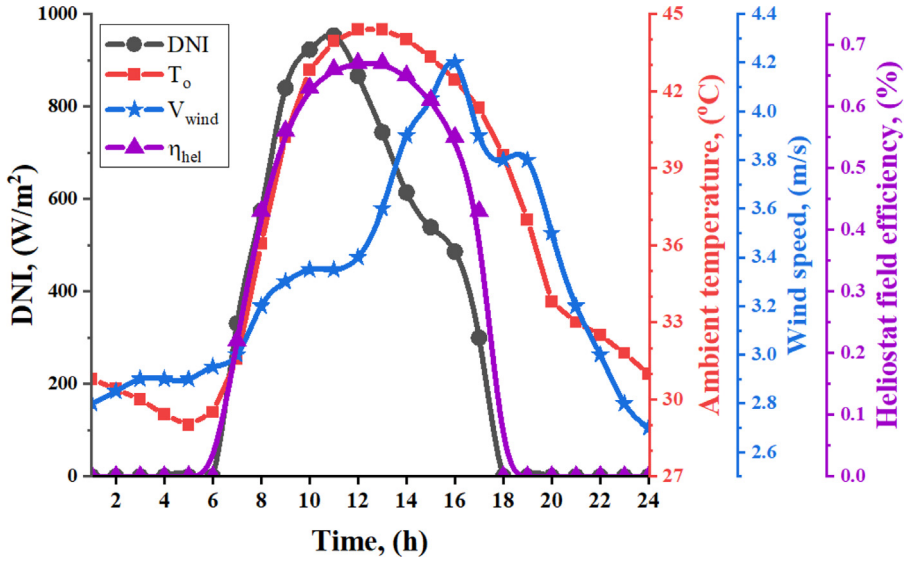

Fig. 8. Ambient conditions are used in the design of the CSP system of the proposed system.

Table 5
Effect of the molten salt type on the performance of the proposed system.

HTF	Salt type	T_{LL}[a] [°C]	T_{UL}[a] [°C]	T_{max} [°C]	$\dot{m}_{CO2}$ [kg/s]	Q_{heater} [MW]	LCOE [¢/kWh]	η_{sCO2} [%]
MS1	0.6NaNO3_0.4KNO3	260	593	550	1156	334.33	13.37	40.54
MS2	0.8NaF_0.92NaBF4	385	696	650	986.9	321.55	12.99	42.15
MS3	0.67LiF_0.33BeF2	477	827	750	863.6	315.24	12.84	42.99

[a] T_{LL}: Lower limit temperature; T_{UL}: Upper limit temperature.

and makes it more reliable for power generation even on cloudy days or in the winter season. The only drawback of Case-5 is its large CO_2 emissions compared to the other cases as will be discussed in Section 5.5. Thus, Cases 2 or 3 can be considered as more suitable cases from both economic and environmental points of view. For instance, Case-2 reduces the LCOE by 22% compared to 30% for Case-5. However, the AH provides only 15% of the daily energy demand, which significantly minimizes CO_2 emissions while maintaining the LCOE at a competitive level for Case-5. Therefore, Case-2 and Case-5 are selected for further investigation at optimized operating conditions (Section 5.5).

As the performance of the sCO_2 power cycle depends on the maximum temperature T_{max} at the inlet of the turbine, three different molten salt types (shown in Table 5) are considered to accommodate the desired range of T_{max} for the present sCO_2 power cycle (550 °C–750 °C). Each molten salt is tested at T_{max} (Table 5) that is within the safety margin from its upper-temperature limit (for MS1: T_{max} = 550 °C, MS2: T_{max} = 650 °C, MS3: T_{max} = 750 °C). At higher turbine inlet temperatures, the mass flow rate of the sCO_2 is reduced as the power capacity is fixed at 135 MW. Consequently, the heater load is reduced too, which improves the sCO_2 efficiency by 3.97% at T_{max} = 650 °C and by 6.04% at T_{max} = 750 °C relative to its value at T_{max} = 550 °C.

5.3. Economic comparison

To assess the economic feasibility of the investigated cases to drive the C3MR LNG process, it is essential to compare the LCOE of the present CSP-sCO_2 power system to that of other energy generation technologies. Fig. 10 compares the maximum, minimum, and median LCOEs of renewable energy and fossil-fuel technologies (Timilsina, 2021; Lazard, 2019; Taylor et al., 2020). As the capacity factor of the stand-alone CSP power system is varying between 32% to 68% (Timilsina, 2021), their LCOE is relatively high compared to fossil-fuel-based technologies. Although some modern CSP projects with TES have guaranteed LCOE of less than 10 ¢/kWh (e.g. the LCOE of SUPCON Delingha 50 MW Tower CSP Project is 9 ¢/kWh (National Renewable Energy Laboratory, 2020b)), it is still higher than the minimum values of the other technologies (see Fig. 10, blue bars). In addition, other CSP projects have high LCOE that exceeds 14 ¢/kWh (e.g. the LCOE of the NOOR III CSP project is 15 ¢/kWh (National Renewable Energy Laboratory, 2020a)). Therefore, the median LCOE of the concentrated solar power tower (SPT) system is higher than the other technologies except for offshore wind.

But, from a technical point of view, the CSP technology is more attractive for clean power generation at high capacity. On one hand, the availability of solar energy is higher than other renewable sources in most LNG-producing countries. On the other hand, using solar PV to drive the C3MR process will need additional electric motors and large storage capacities, which are not included in the calculations of the solar PV LCOE presented in Fig. 10. To reach a competitive level for fossil-fuel technologies, the hybridization of the CSP with AH driven by the flash-gas from the C3MR process is an attractive option as discussed in the next subsection.

The economic performance of the present CSP-sCO_2 power system is compared to the other real CSP-Steam power systems that work at medium to large power scale as presented in Supplementary material B (Table SB.7). In addition, the economic performance of a CSP-steam Rankine power system at a power capacity of 135 MW_e is generated using Greenius software (Dersch et al., 2008). First, the Greenius results were validated against a real CSP power plant (as presented in Supplementary material B (Table SB.3 and Table SB.4)). Then, the environmental data for Ras Laffan (Qatar's main site for the production of LNG) are imported to the model and the power block specifications are scaled down to match the desired capacity of the present work (135 MW_e). The results show that the LCOE of the steam-based cycle (14.16 ¢/kWh, calculated using Greenius software) is lower than that of Case-1 (14.87 ¢/kWh) by 4.7% under dry-cooling conditions. But Case-2 and Case-5 have LCOE of 11.98 ¢/kWh and 10.15 ¢/kWh, respectively. This means that Case-2 and Case-5 reduce the LCOE by 15.4% and 28.3% compared to the steam-based system, respectively. The LCOE of the two first CSP power plants in Table SB. 7 (LuNeng Haixi and Shouhang Dunhuang Phase II), which

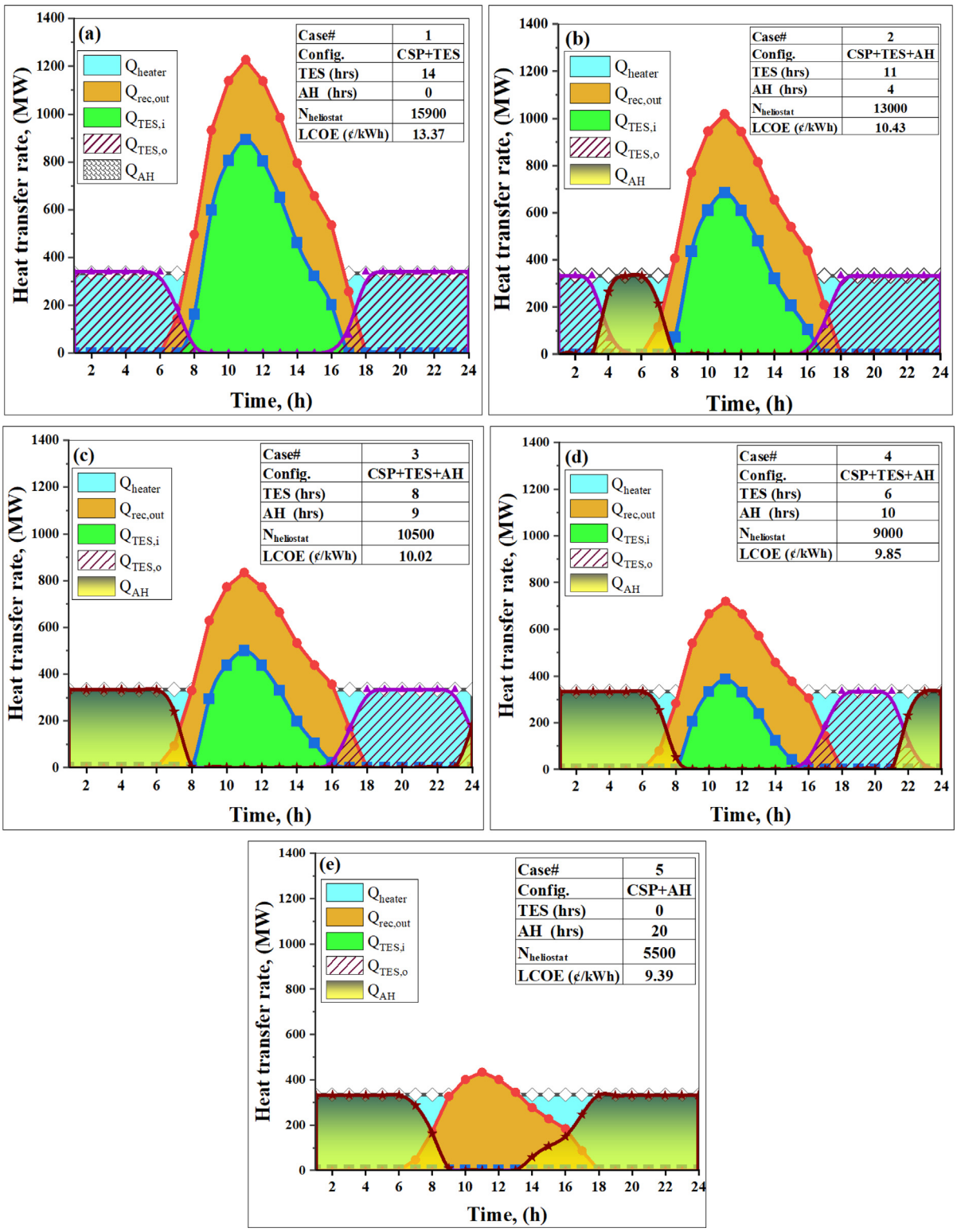

Fig. 9. Thermal power transfer mechanisms of the proposed cases for the integration between the C3MR LNG process and the CSP sCO_2 power system.

were built in China, is less than those built in the USA (Crescent Dunes and Ivanpah Solar) or Morocco (NOOR III) by an average of 51%. Also, it is cheaper than the present CSP-sCO_2-based plant by an average of 31%. This may be returned to that China built up a domestic industry capable of building stations and most components at lower costs than foreign competitors (Lilliestam et al., 2019).

For the integrated CSP-sCO_2 power system, the payback period (PBP) can be defined in terms of the LCOE, plant lifetime (n), power purchasing agreement (PPA), and the plant utilization factor (PUF) as (Omar et al., 2021):

$$PBP = \frac{LCOE \times n}{PPA \times PUF} \tag{35}$$

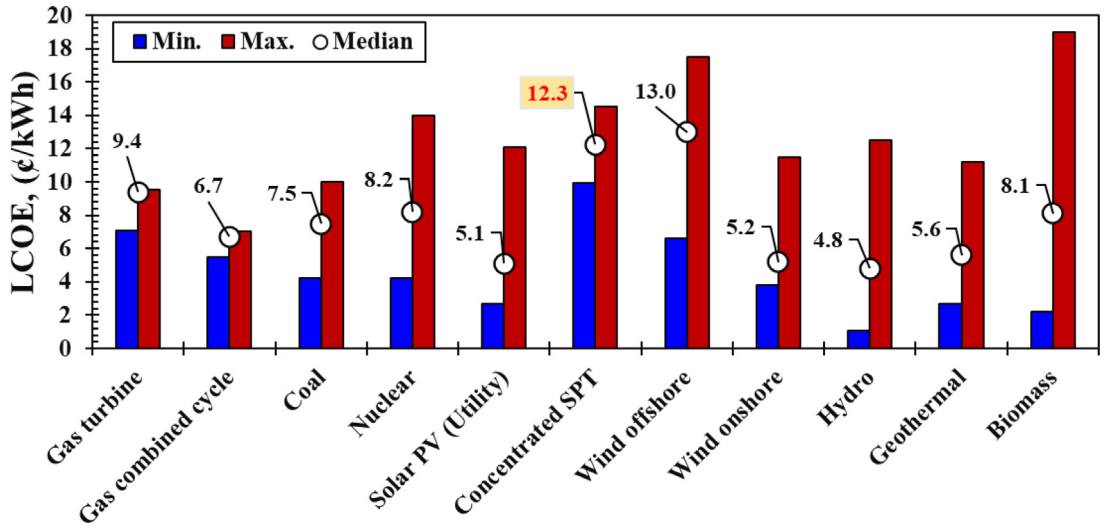

Fig. 10. LCOE of the concentrated solar power tower system compared to other power technologies. . (For interpretation of the references to color in this figure legend, the reader is referred to the web version of this article.)

Table 6
Comparison between the economic performance indicators of the present CSP-sCO_2 power system and other systems available in the literature (At *PPA* = 20 ¢/kWh, *n* = 25 years, *PUF* = 96%)[a].

Ref.	System configuration	Net output power (MW)	LCOE (¢/kWh)	PBP (years)
Omar et al. (2021)	CSP-sCO_2-MED	50	11.20	14.58
Ma et al. (2018)	CSP-sCO2-AC	10	13.72	14.44
Present study	CSP+TES (Case-1)	135	13.37	17.41
Present study	CSP+TES+AH (Case-2)	135	10.43	13.58
Present study	CSP+AH (Case-5)	135	9.39	12.23

[a]MED = Multi-effect distillation, AC = Absorption chiller.

The LCOE and PBP economic indicators of the proposed CSP-sCO_2 power system (Case-1, Case-2, and Case-5) are compared with those reported for similar systems available in the literature as shown in Table 6. It can be noted that Case-2 and Case-5 of the present CSP-sCO2 system achieve lower LCOE and PBP than other CSP-sCO_2 systems in Omar et al. (2021) and (Ma et al., 2018). In particular, Case-5 has a LCOE of 9.39, which is 32% lower than the system in Ma et al. (2018) and 16% than in Omar et al. (2021). In addition, its PBP is 2 years lower than that of both systems in Omar et al. (2021) and Ma et al. (2018). This is explained by that the present system has larger net output power and the recovery of the flash-gas minimizes or eliminates the need for the thermal energy storages of the CSP system. This emphasizes the economic feasibility of the present system especially if the locations of the C3MR process and CSP filed are relatively close.

5.4. Sensitivity analysis of the sCO_2 power cycle

The sensitivity analysis of the major operating conditions of the sCO2 power cycle is performed and presented in Supplementary material C. As Case-3 has an almost equal contribution for the TES and AH, it was selected as the reference case for the present sensitivity analysis. Also, the analysis is performed at the power capacity of the C3MR process (Composition 1). The analyzed parameters include the maximum cycle pressure (as shown in Supplementary material C (Fig. SC.1, Fig. SC.1)), minimum cycle pressure (Fig. SC.2), intermediate pressure ratio (Fig. SC.3), and minimum cycle temperature (Fig. SC.4). In addition, the effect of the maximum cycle temperature was investigated alongside each of the aforementioned parameters. From the sensitivity analysis, it is found that there are optimal values for the maximum, minimum, and intermediate cycle pressures. In addition, the performance of the cycle at wet-cooling conditions is superior compared to dry-cooling conditions. Moreover, there are trade-offs between the cycle efficiency and the LCOE, especially with the variation of the minimum cycle pressure. Thus, an optimization study is conducted in Section 5.5 to optimize the performance of the overall system.

5.5. Optimization analysis

In this section, the operating parameters of both the C3MR process and the sCO_2 power cycle are optimized to achieve the best energetic, exergetic, and economic performance of the CSP-sCO_2 system. The decision variables of the C3MR process and their optimization range are presented in Supplementary material (Table SB. 8). Two objective functions are considered for the optimization process of the C3MR process, which are maximizing the produced LNG (Max. LNG flow) or minimizing the compression power of the C3MR process (Min. Compr. Power). The optimized parameters by each function are also presented in (Table SB.8). The LNG flow, compression power, and the COP of the C3MR obtained by each optimization function are presented in Table 7. Compared to the original values of these output parameters (before optimization), it is noted that the "Max. LNG flow" function enhances the LNG flow by 7.4 kg/s. However, the compression power (for the same function), is increased by 2.4 MW. Similarly, the "Min. Compr. Power" reduced the compression power by 3.8 MW, however, the LNG flow is also reduced by 8.5 kg/s. Thus, the optimization results for the "Max. LNG flow" is best fit for Case-2 as the requirement for the flash-gas is minimal while the results of "Min. Compr. Power" is best fit for Case-5 as high flash-gas flow is needed for 20 h/day as discussed in Section 5.2. Therefore, Case-2 and Case-5 are selected for further optimization analysis for the operating parameters of the sCO_2 cycle as explained in the next subsection.

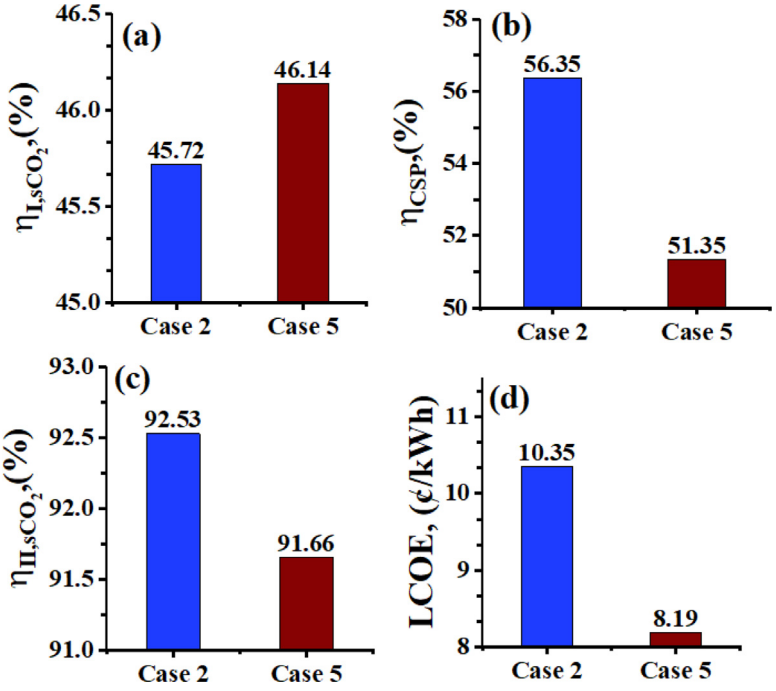

Fig. 11. Comparison between the optimized performance indicators for sCO2 power cycle by MOF for (a) Case-2 (CSP+TES+AH), and (b) Case-5 (CSP+AH).

Table 7
Optimization results of the C3MR LNG process.

Optimized function	Original values	Optimized by "Max. LNG Flow" function	Optimized by "Min. Compr. Power" function
LNG flow, (kg/s)	119.9	127.3	111.4
Compression power, (MW)	127.4	129.8	123.6
COP	2.32	1.558	2.171

The optimization analysis of the sCO_2 power cycle is performed using the genetic algorithm tool available in the EES library with a mutation rate of 0.2625, a number of generations of 64, and a number of individuals of 16. Five operational parameters are selected to be optimized: P_{max} within the range (200 to 300 bar), P_{min} (75 to 85 bar), T_{max} (550 to 750 °C), T_{min} (32–50 °C), and IPR (0.2–0.6). The optimization process is conducted using three single objective functions (SOFs): maximizing the energy efficiency (Max. $\eta_{I,sCO2}$), maximizing the exergy efficiency (Max. $\eta_{II,sCO2}$), and minimizing the LCOE (Min. LCOE). The optimized decision variables and the corresponding values of the objective functions are presented in Table 8. It is noted that there is a trade-off between the decision variables for the optimum energy efficiency, exergy efficiency, and the LCOE. Therefore, a multi-objective function (MOF) is used to find the optimal decision for these three objective functions. The MOF is defined as

$$Max.MOF = w_1 \times \eta_{I,sCO2} + w_2 \times \eta_{II,sCO2} + w_3 \times \left(1 - \frac{LCOE}{LCOE_{ref}}\right) \quad (36)$$

where w_1, w_2, and w_3 are the weighting coefficients of $\eta_{I,sCO2}$, $\eta_{II,sCO2}$, and $LCOE$, respectively. $LCOE_{ref}$ is the reference value of the LCOE used to normalize the third term of the MOF. It was set equal to the median LCOE of the CSP technology (13 ¢/kWh) as reported by Timilsina (2021). In this work, the three objective functions are of the same importance, therefore, the weighting coefficients are assumed to be the same ($w_1 = w_2 = w_3 = 1/3$). This equal-weight approach is recommended by some optimization studies such as in Sleiti et al. (2021b) and Alharbi et al. (2020).

Fig. 11 compares the values of the objective functions obtained by the MOF for both Case-2 and Case-3 of the present work with the corresponding values of the CSP efficiency (Fig. 11(b)). It can be noted that the energetic and exergetic performance of Case-5 is superior to that of Case-2. This means that the optimization of C3MR for minimizing the power alongside the CSP integration without TES (Case-5) brings the LCOE to 8.19 ¢/kWh which is lower than the median LCOE of gas turbines (9.4 ¢/kWh) and competitive with coal technology (7.5 ¢/kWh). In conclusion, Case-5 eliminates the TES and reduced the number of heliostats by 42% compared to Case-2. Also, the continuous operation of the AH in Case-5 for 20 h/day minimizes the size of the storage tank of the flash-gas. Thus, Case-5 is the best economic choice among the other proposed cases. However, the disadvantage of Case-5 is its large CO_2 emissions compared to the other cases as discussed in the next section. Therefore, if the reduction of CO_2 emissions is limited by strict environmental laws, Case-2 is the best-fit alternative for Case-5 as it minimizes the CO_2 emissions with LCOE of 10.35 ¢/kWh. Although this LCOE is still higher than that of the gas turbines by 10%, the CO_2 emissions of Case-2 are decreased by 86% compared to gas turbines under the same power capacity.

Before proceeding to the environmental analysis, it is worth explaining the exergetic performance of Case-2 and Case-5 under the MOF optimized conditions, Fig. 12. The Sankey diagrams of the exergy flow for Case-2 (Fig. 12(a)) and Case-5 (Fig. 12 (b)) reveal that the overall exergy performance of Case-5 is higher than that of Case-2 by 2.1%. This returns to that the exergy input to the heater in Case-5 is lower than that of Case-2, which increases the exergy destruction rate. At the components level, the largest portion of the exergy destruction occurs in the LTR and HTR, therefore, further improvements for these components are needed.

5.6. Environmental analysis

The annual CO_2 avoidance due to the utilization of solar energy is calculated by subtracting the energy provided by the auxiliary

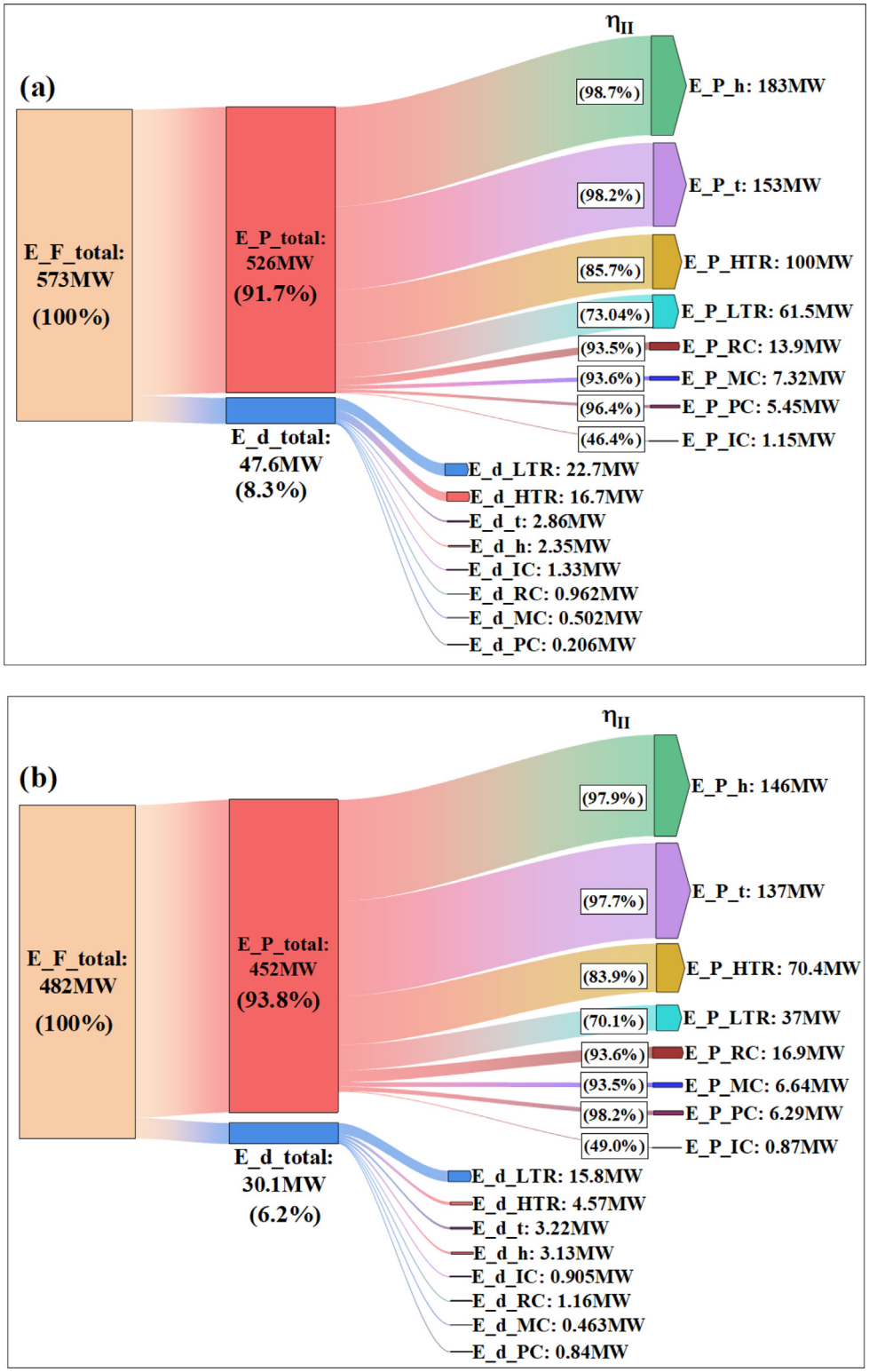

Fig. 12. Exergy flow of the sCO_2 power cycle at (a) Case-2 (CSP+TES+AH), and (b) Case-5 (CSP+AH).

heater (which produced CO_2) from the total energy demand of the system. The result will be the energy provided by the CSP system, which is carbon-free energy. Then, multiply the result by the amount of CO2 emitted from the combustion of flash-gases to get the amount of avoided CO_2 emissions (Mokheimer et al., 2017):

$$CO2_{Saved} = (E_{demand} - E_{AH,fuel}) \times f_{CO_2} \quad (37)$$

where E_{demand} is the annual energy demand of the C3MR system, $E_{AH,fuel}$ is the annual energy generated by the AH using the flash-gas, and f_{CO_2} is the amount of CO_2 emissions, which is set as $f_{CO_2} = 0.055$ kg-CO_2/MJ (Mokheimer et al., 2017). The reduction percentage is defined as:

$$\Delta CO_2(\%) = 100 \times (CO2_{Ref} - CO2_{AH,fuel})/CO2_{Ref} \quad (38)$$

Table 8
Optimization results of the sCO_2 power cycle.

Case #	Opt. function	Decision variables					Results		
		P_{max} [bar]	P_{min} [bar]	T_{max} [°C]	T_{min} [°C]	IPR [–]	$\eta_{I,sCO2}$ [%]	$\eta_{II,sCO2}$ [%]	LCOE [¢/kWh]
2	Max.$\eta_{I,sCO2}$	300.00	77.04	744.70	32.45	0.54	46.47	91.77	10.28
	Max.$\eta_{II,sCO2}$	289.80	76.30	552.30	32.43	0.60	43.00	93.63	10.60
	Min.LCOE	300.00	75.75	750.00	32.00	0.60	46.81	91.84	10.25
	Max.MOF	300.00	76.72	671.40	32.41	0.55	45.72	92.53	10.35
5	Max.$\eta_{I,sCO2}$	299.10	76.65	747.90	32.37	0.58	46.54	91.62	8.19
	Max.$\eta_{II,sCO2}$	300.00	76.64	550.00	32.00	0.60	43.56	93.92	8.30
	Min.LCOE	300.00	75.00	750.00	41.16	0.60	44.07	90.65	8.17
	Max.MOF	300.00	78.68	736.40	32.44	0.59	46.14	91.66	8.20

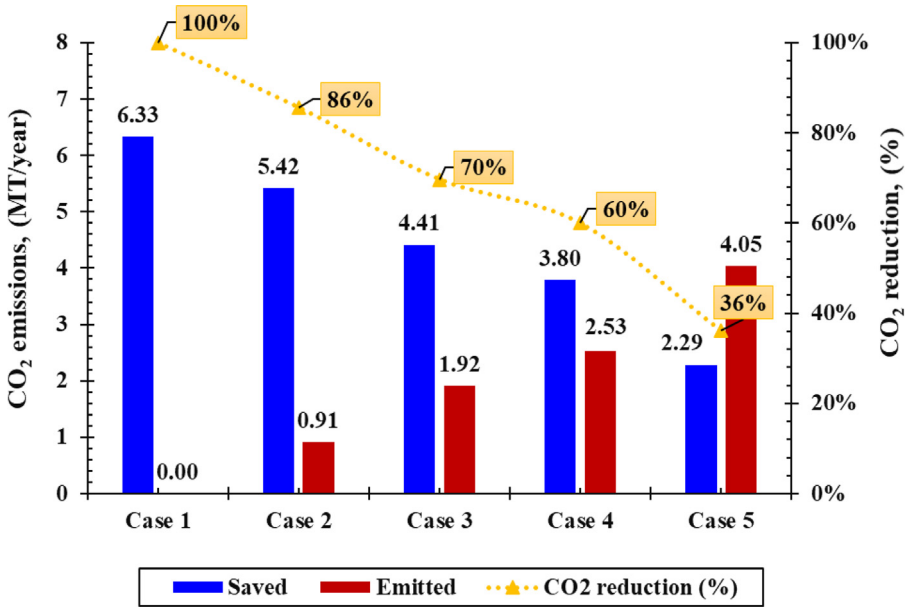

Fig. 13. Comparison of annual CO_2 emissions from the hybrid C3MR CSP-sCO_2 cases.

Fig. 13 shows the annual amount of emitted and saved CO_2 per case. Case-1 can be considered as the reference case of the avoided CO_2 emissions compared to the C3MR process driven by fossil fuel (NG). As Case-5 shows the best economic performance with LCOE of 8.19 ¢/kWh, its CO_2 is the highest compared to the other cases. However, it reduces the CO_2 emittance by 36% compared to Case-1. Compared to the total annual CO_2 emissions in Qatar (104 MT/year (Alns and Sleiti, 2021)), Case-1 reduces the total CO_2 emissions by 6.08% while Case-5 reduces it by 2.20%. Therefore, Case-5 has a simpler structure than the other cases and competitive economic performance compared to conventional fossil-fuel power plants. With optimal environmental analysis, it may be recommended to be implemented with the C3MR process. If the priority is given to the CO_2 emissions reduction, Case-2 is the best suited with LCOE of 10.13 ¢/kWh and CO_2 reduction of 5.2%.

6. Conclusions

This work presents a novel integration between the C3MR LNG process and the CSP-sCO_2 power cycle. The hybrid system utilizes the solar energy of the CSP system and the flash-gas of the C3MR process to drive an intercooled sCO_2 power block. First, the cold energy of the flash-gas is used in the precooling process of the sCO_2 cycle. Then, the flash-gas is stored and used to support the CSP field using an auxiliary heater (AH). The proposed system reduces the CSP field size, eliminates or reduces the need for TES, and utilizes a more efficient and compact power block than the steam Rankine cycle. Five different integration cases were examined in this study, including Case-1 where the sCO_2 power block is driven by the CSP and its TES without the use of an AH; Cases 2 to 4, where the sCO_2 power block is driven by the CSP with both TES and AH, with different contributions of the TES and AH; and Case-5, where the sCO_2 power block is driven by the CSP and AH without TES. The proposed system was evaluated using thorough energetic, exergetic, economic, and environmental analyses. The main findings are:

- The proposed system achieves lower LCOE (by 15.4% (Case-2) to 28.3% (Case-5) than the steam-based CSP system.
- The proposed system can eliminate CO_2 emissions in Case-1 or at least reduce them by 36% in Case-5, making it highly beneficial for decarbonization strategies in LNG processes.
- Optimization analysis reduces the LCOE of Case-2 and Case-5 to 10.35 ¢/kWh and 8.19 ¢/kWh, respectively, while significantly reducing CO2 emissions.
- The LTR and HTR have the largest share in the exergy destruction; thus, these components need further improvements to enhance the overall performance of the power block.
- The proposed system reduces the total annual CO_2 emissions by 5.5% in Case-2 to 2.2% in Case-5 at the designed capacity (135 MWe, 130 kg-NG/s).

Future work should investigate the proposed system at off-design conditions and different capacities for the LNG process. A comprehensive comparison of the present system with other systems in the literature under the same operating conditions is also recommended to confirm the superior performance of the proposed system. Overall, the integration of the C3MR LNG process and the CSP-sCO2 power cycle offers a promising solution to the challenges of energy-intensive processes with large CO_2 emissions.

CRediT authorship contribution statement

Ahmad K. Sleiti: Conceptualization, Investigation, Writing – original draft, Writing – review & editing, Resources, Formal analysis, Project administration, Funding acquisition, Supervision. **Wahib A. Al-Ammari:** Conceptualization, Writing – original draft, Investigation, Software, Data curation, Validation, Formal analysis.

Declaration of competing interest

The authors declare that they have no known competing financial interests or personal relationships that could have appeared to influence the work reported in this paper.

Data availability

The data of the article are provided in a supplementary material.

Acknowledgment

The work presented in this publication was made possible by NPRP-S grant # [11S-1231-170155] from the Qatar National Research Fund (a member of Qatar Foundation). The findings herein reflect the work, and are solely the responsibility, of the authors.

Appendix A. Supplementary data

Supplementary material related to this article can be found online at https://doi.org/10.1016/j.egyr.2023.04.012.

References

Afrouzy, ZA., Taghavi, M., 2021. Thermo-economic analysis of a novel integrated structure for liquefied natural gas production using photovoltaic panels. J. Therm. Anal. Calorim. 145, 1509–1536. http://dx.doi.org/10.1007/s10973-021-10769-4.

Al-Mutaz, IS., Liu, X., Mazza, G., 2016. Natural gas liquefaction technologies - An overview. Oil Gas Eur. Mag. 42, 213–218.

Alharbi, S., Elsayed, ML., Chow, LC., 2020. Exergoeconomic analysis and optimization of an integrated system of supercritical CO2 brayton cycle and multi-effect desalination. Energy 197, 117225. http://dx.doi.org/10.1016/j.energy.2020.117225.

Allahyarzadeh-Bidgoli, A., Dezan, DJ., Yanagihara, JI., 2020. COP optimization of propane pre-cooling cycle by optimal fin design of heat exchangers: Efficiency and sustainability improvement. J. Clean. Prod. 271, 122585. http://dx.doi.org/10.1016/j.jclepro.2020.122585.

Almeida Trasviña, HF., 2016. Development of novel refrigeration cycles for small scale LNG processes. Fac. Eng. Phys. Sci. Sch. Chem. Eng. Anal. Sci. Master of, 175.

Almeida-Trasvina, F., Smith, R., 2018. Design and Optimisation of Novel Cascade Refrigeration Cycles for LNG Production, Vol. 43. Elsevier Masson SAS, http://dx.doi.org/10.1016/B978-0-444-64235-6.50111-X.

Alns, A., Sleiti, AK., 2021. Combined heat and power system based on solid oxide fuel cells for low energy commercial buildings in Qatar. Sustain. Energy Technol. Assess. 48, 101615. http://dx.doi.org/10.1016/j.seta.2021.101615.

Ansarinasab, H., Mehrpooya, M., 2017. Advanced exergoeconomic analysis of a novel process for production of LNG by using a single effect absorption refrigeration cycle. Appl. Therm. Eng. 114, 719–732. http://dx.doi.org/10.1016/j.applthermaleng.2016.12.003.

Bin Omar, MN., Morosuk, T., Tsatsaronis, G., 2014. Thermodynamic and economic evaluation of a novel mixed-refrigerant process for the liquefaction of natural gas. In: Proc. ASME 2014 Int. Mech. Eng. Congr. Expo. pp. 1–11. http://dx.doi.org/10.1115/IMECE2014-39639.

2022. Countries with largest liquefied natural gas (LNG) export capacity in operation worldwide as of 2021. Chem. Resour. Fuels https://www.statista.com/statistics/1262074/global-lng-export-capacity-by-country/ (accessed June 6, 2022).

Cycle, P., Soujoudi, R., R., Manteufel, 2021. Thermodynamic, economic and environmental analyses of ammonia-based mixed refrigerant for liquefied natural gas pre-cooling cycle. Processes 9, 1298. http://dx.doi.org/10.3390/pr9081298.

Dersch, J., Hennecke, K., Quaschning, V., 2008. Greenius – A simulation tool for renewable energy utilisation. In: EUROSUN 2008 First Int Congr Heating, Cool Build. p. 8.

Elbeh, MB., Sleiti, AK., 2021. Analysis and optimization of concentrated solar power plant for application in arid climate. Energy Sci. Eng. 9, 784–797. http://dx.doi.org/10.1002/ese3.742.

Furda, P., Variny, M., Labovská, Z., 2022. Towards time-effective optimization: Enviro-economic study of the C3MR LNG process. Energy Convers. Manage. 260. http://dx.doi.org/10.1016/j.enconman.2022.115602.

Ghorbani, B., Hamedi, MH., Shirmohammadi, R., Hamedi, M., Mehrpooya, M., 2016. Exergoeconomic analysis and multi-objective Pareto optimization of the C3MR liquefaction process. Sustain. Energy Technol. Assess. 17, 56–67. http://dx.doi.org/10.1016/j.seta.2016.09.001.

Ghorbani, B., Rahnavard, Z., Ahmadi, MH., Jouybari, AK., 2021. An innovative hybrid structure of solar PV-driven air separation unit, molten carbonate fuel cell, and absorption–compression refrigeration system (Process development and exergy analysis). Energy Rep. 7, 8960–8972. http://dx.doi.org/10.1016/j.egyr.2021.10.108.

He, T., Lin, W., 2020. Energy saving research of natural gas liquefaction plant based on waste heat utilization of gas turbine exhaust. Energy Convers. Manage. 225, 113468. http://dx.doi.org/10.1016/j.enconman.2020.113468.

He, T., Lin, W., 2021. Design and analysis of dual mixed refrigerant processes for high-ethane content natural gas liquefaction. Chinese J. Chem. Eng. 29, 354–364. http://dx.doi.org/10.1016/j.cjche.2020.09.019.

Jin, C., Yuan, Y., Son, H., Lim, Y., 2022. Novel propane-free mixed refrigerant integrated with nitrogen expansion natural gas liquefaction process for offshore units. Energy 238, 121765. http://dx.doi.org/10.1016/j.energy.2021.121765.

Lazard, 2019. Levelized cost of energy and levelized cost of storage. LazardCom 1–20.

Lee, I., Park, J., Moon, I., 2018. Key issues and challenges on the liquefied natural gas value chain: A review from the process systems engineering point of view. Ind. Eng. Chem. Res. 57, 5805–5818. http://dx.doi.org/10.1021/acs.iecr.7b03899.

Lilliestam, J., Ollier, L., Pfenninger, S., 2019. The dragon awakens: Will China save or conquer concentrating solar power? AIP Conf. Proc. 2126. http://dx.doi.org/10.1063/1.5117648.

Lim, W., Lee, I., Tak, K., Cho, JH., Ko, D., Moon, I., 2014. Efficient configuration of a natural gas liquefaction process for energy recovery. Ind. Eng. Chem. Res. 53, 1973–1985. http://dx.doi.org/10.1021/ie4003427.

Luo, D., Huang, D., 2020. Thermodynamic and exergoeconomic investigation of various SCO2 Brayton cycles for next generation nuclear reactors. Energy Convers. Manage. 209, 112649. http://dx.doi.org/10.1016/j.enconman.2020.112649.

Ma, Y., Morosuk, T., Luo, J., Liu, M., Liu, J., 2020. Superstructure design and optimization on supercritical carbon dioxide cycle for application in concentrated solar power plant. Energy Convers. Manage. 206, 112290. http://dx.doi.org/10.1016/j.enconman.2019.112290.

Ma, Y., Zhang, X., Liu, M., Yan, J., Liu, J., 2018. Proposal and assessment of a novel supercritical CO2 brayton cycle integrated with LiBr absorption chiller for concentrated solar power applications. Energy 148, 839–854. http://dx.doi.org/10.1016/j.energy.2018.01.155.

Mackenzie, W., 2021. Renewable energy could reduce Asia Pacific LNG plant emissions by 8% 2020. https://www.woodmac.com/press-releases/renewable-energy-could-reduce-asia-pacific-lng-plant-emissions-by-8/ (accessed October 18, 2021).

Mazyan, WI., Ahmadi, A., Ahmed, H., Hoorfar, M., 2020. Increasing the COP of a refrigeration cycle in natural gas liquefaction process using refrigerant blends of propane-NH3, propane-SO2 and propane-CO2. Heliyon 6, e04750. http://dx.doi.org/10.1016/j.heliyon.2020.e04750.

Mehrpooya, M., Bahramian, P., Pourfayaz, F., Katooli, H., Delpisheh, M., 2021. A novel hybrid liquefied natural gas process with absorption refrigeration integrated with molten carbonate fuel cell. Int. J. Low-Carbon Technol. 16, 956–976. http://dx.doi.org/10.1093/ijlct/ctab021.

Mehrpooya, M., Omidi, M., Vatani, A., 2016. Novel mixed fluid cascade natural gas liquefaction process configuration using absorption refrigeration system. Appl. Therm. Eng. 98, 591–604. http://dx.doi.org/10.1016/j.applthermaleng.2015.12.032.

Mokhatab, S., Mak, JY., Valappil, J.V., Wood, DA., 2014. Handbook of Liquefied Natural Gas. Elsevier Inc, http://dx.doi.org/10.1016/C2011-0-07476-8.

Mokheimer, EMA., Dabwan, YN., Habib, MA., 2017. Optimal integration of solar energy with fossil fuel gas turbine cogeneration plants using three different CSP technologies in Saudi Arabia. Appl. Energy 185, 1268–1280. http://dx.doi.org/10.1016/j.apenergy.2015.12.029.

National Renewable Energy Laboratory, 2020a. NOOR III CSP project. Conc. Sol. Power Proj. https://solarpaces.nrel.gov/project/noor-iii (accessed June 6, 2022).

National Renewable Energy Laboratory, 2020b. SUPCON delingha 50 MW tower CSP project. Conc. Sol. Power Proj. https://solarpaces.nrel.gov/project/supcon-delingha-50-mw-tower (accessed June 6, 2022).

National Renewable Energy Laboratory, 2022. Concentrating solar power project 2020. https://solarpaces.nrel.gov/by-country (accessed June 6, 2022).

Omar, A., Saldivia, D., Li, Q., Barraza, R., Taylor, RA., 2021. Techno-economic optimization of coupling a cascaded MED system to a CSP-sCO2 power plant. Energy Convers. Manage. 247, 114725. http://dx.doi.org/10.1016/j.enconman.2021.114725.

Park, J., You, F., Mun, H., Lee, I., 2021. Liquefied natural gas supply chain using liquid air as a cold carrier: Novel method for energy recovery. Energy Convers. Manage. 227, 113611. http://dx.doi.org/10.1016/j.enconman.2020.113611.

Primabudi, E., Morosuk, T., Tsatsaronis, G., 2019. Multi-objective optimization of propane pre-cooled mixed refrigerant (C3MR) LNG process. Energy 185, 492–504. http://dx.doi.org/10.1016/j.energy.2019.07.035.

Qyyum, MA., He, T., Qadeer, K., Mao, N., Lee, S., Lee, M., 2020. Dual-effect single-mixed refrigeration cycle: An innovative alternative process for energy-efficient and cost-effective natural gas liquefaction. Appl. Energy 268, 115022. http://dx.doi.org/10.1016/j.apenergy.2020.115022.

Rajabloo, T., Valee, J., Marenne, Y., Coppens, L., De Ceuninck, W., 2023. Carbon capture and utilization for industrial applications. Energy Rep. 9, 111–116. http://dx.doi.org/10.1016/j.egyr.2022.12.009.

Reyes-Belmonte, MA., Sebastián, A., González-Aguilar, J., Romero, M., 2017. Performance comparison of different thermodynamic cycles for an innovative central receiver solar power plant. AIP Conf. Proc. 1850. http://dx.doi.org/10.1063/1.4984558.

Rogalev, A., Grigoriev, E., Kindra, V., Rogalev, N., 2019. Thermodynamic optimization and equipment development for a high efficient fossil fuel power plant with zero emissions. J. Clean. Prod. 236, 117592. http://dx.doi.org/10.1016/j.jclepro.2019.07.067.

Sanavandi, H., Ziabasharhagh, M., 2016. Design and comprehensive optimization of C3MR liquefaction natural gas cycle by considering operational constraints. J. Nat. Gas Sci. Eng. 29, 176–187. http://dx.doi.org/10.1016/j.jngse.2015.12.055.

Santos, LF., Costa, CBB., Caballero, JA., Ravagnani, Mass, 2021. Kriging-assisted constrained optimization of single-mixed refrigerant natural gas liquefaction process. Chem. Eng. Sci. 241, 116699. http://dx.doi.org/10.1016/j.ces.2021.116699.

Scaccabarozzi, R., Gatti, M., Martelli, E., 2016. Thermodynamic analysis and numerical optimization of the NET Power oxy-combustion cycle. Appl. Energy 178, 505–526. http://dx.doi.org/10.1016/j.apenergy.2016.06.060.

Scaccabarozzi, R., Gatti, M., Martelli, E., 2017. Thermodynamic optimization and part-load analysis of the NET power cycle. Energy Procedia 114, 551–560. http://dx.doi.org/10.1016/j.egypro.2017.03.1197.

Shazed, AR., Ashraf, HM., Katebah, MA., Bouabidi, Z., Al-musleh, EI., 2021. Overcoming the energy and environmental issues of LNG plants by using solid oxide fuel cells. Energy 218, 119510. http://dx.doi.org/10.1016/j.energy.2020.119510.

Sleiti, AK., Al-Ammari, WA., 2021. Energy and exergy analyses of novel supercritical CO2 Brayton cycles driven by direct oxy-fuel combustor. Fuel 294, 120557. http://dx.doi.org/10.1016/j.fuel.2021.120557.

Sleiti, AK., Al-ammari, WA., 2021. Off-design performance analysis of combined CSP power and direct oxy-combustion supercritical carbon dioxide cycles. Renew. Energy 180, 14–29. http://dx.doi.org/10.1016/j.renene.2021.08.047.

Sleiti, AK., Al-ammari, WA., 2022. Systematic thermodynamic approach for designing mixed refrigerants used in hydrogen precooling process. Int. J. Hydrog. Energy 47, 20915–20931. http://dx.doi.org/10.1016/j.ijhydene.2022.04.233.

Sleiti, AK., Al-Ammari, WA., Aboueata, KM., 2022. Flare gas-to-power by direct intercooled oxy-combustion supercritical CO2 power cycles. Fuel 308, 121808. http://dx.doi.org/10.1016/j.fuel.2021.121808.

Sleiti, AK., Al-Ammari, W., Ahmed, S., Kapat, J., 2021a. Direct-fired oxy-combustion supercritical-CO2 power cycle with novel preheating configurations -thermodynamic and exergoeconomic analyses. Energy 226, 120441. http://dx.doi.org/10.1016/j.energy.2021.120441.

Sleiti, AK., Al-Ammari, WA., Vesely, L., Kapat, JS., 2021b. Thermoeconomic and optimization analyses of direct oxy-combustion supercritical carbon dioxide power cycles with dry and wet cooling. Energy Convers. Manage. 245, 114607. http://dx.doi.org/10.1016/j.enconman.2021.114607.

Sleiti, AK., Al-Ammaria, WA., 2022. Combined direct oxy-combustion and concentrated solar supercritical carbon dioxide power system – Thermo, exergoeconomic and quadruple optimization analyses. Int. J. Energy Res. 46, 9560–9585. http://dx.doi.org/10.1002/er.7825.

Sun, H., Geng, J., Na, F., Rong, G., Wang, C., 2022. Performance evaluation and comparison of commonly used optimization algorithms for natural gas liquefaction processes. Energy Rep. 8, 4787–4800. http://dx.doi.org/10.1016/j.egyr.2022.03.164.

Sun, H., He Ding, D., He, M., Shoujun Sun, S., 2016. Simulation and optimisation of AP-X process in a large-scale LNG plant. J. Nat. Gas Sci. Eng. 32, 380–389. http://dx.doi.org/10.1016/j.jngse.2016.04.039.

Sun, K., Zhao, T., Wu, S., Yang, S., 2021. Comprehensive evaluation of concentrated solar collector and organic rankine cycle hybrid energy process with considering the effects of different heat transfer fluids. Energy Rep. 7, 362–384. http://dx.doi.org/10.1016/j.egyr.2021.01.004.

Swanson, C., Science Center, ., Levin, A., Stevenson, A., Mall, A., Spencer, T., 2020. Sailing to nowhere: Liquefied natural gas is not an effective climate strategy.

Syblik, J., Vesely, L., Stepanek, J., Entler, S., Dostal, V., 2023. Techno-economic comparison of DEMO power conversion systems. Energy Rep. 9, 2777–2786. http://dx.doi.org/10.1016/j.egyr.2023.01.125.

Taylor, M., Ralon, P., Anuta, H., Al-Zoghoul, S., 2020. Renewable power generation costs in 2019.

Timilsina, GR., 2021. Are renewable energy technologies cost competitive for electricity generation? Renew. Energy 180, 658–672. http://dx.doi.org/10.1016/j.renene.2021.08.088.

Utamura, M., Hasuike, H., Ogawa, K., Yamamoto, T., Fukushima, T., Watanabe, T., et al., 2016. Demonstration of supercritical CO2 closed regenerative Brayton cycle in a bench scale experiment. In: ASME Turbo Expo 2012 Turbine Tech. Conf. Expo. pp. 1–10.

Wang, D., Chen, H., Wang, T., Chen, Y., Wei, J., 2022. Study on configuration of gas-supercritical carbon dioxide combined cycle under different gas turbine power. Energy Rep. 8, 5965–5973. http://dx.doi.org/10.1016/j.egyr.2022.04.037.

Wang, K., He, YL., 2017. Thermodynamic analysis and optimization of a molten salt solar power tower integrated with a recompression supercritical CO2 Brayton cycle based on integrated modeling. Energy Convers. Manage. 135, 336–350. http://dx.doi.org/10.1016/j.enconman.2016.12.085.

Wang, K., He, YL., Zhu, HH., 2017. Integration between supercritical CO2 Brayton cycles and molten salt solar power towers: A review and a comprehensive comparison of different cycle layouts. Appl. Energy 195, 819–836. http://dx.doi.org/10.1016/j.apenergy.2017.03.099.

Wang, M., Khalilpour, R., Abbas, A., 2014. Thermodynamic and economic optimization of LNG mixed refrigerant processes. Energy Convers. Manage. 88, 947–961. http://dx.doi.org/10.1016/j.enconman.2014.09.007.

Wang, K., Li, MJ., Guo, JQ., Li, P., Bin, Z., 2018. A systematic comparison of different S-CO2 Brayton cycle layouts based on multi-objective optimization for applications in solar power tower plants. Appl. Energy 212, 109–121. http://dx.doi.org/10.1016/j.apenergy.2017.12.031.

Wright, S., Scammell, W., Brun, K., Friedman, P., Dennis, R., 2017. Fundamentals and applications of supercritical carbon dioxide (SCO2) based power cycles. Fundam. Appl. Supercrit. Carbon Dioxide Based Power Cycles 127–145. http://dx.doi.org/10.1016/B978-0-08-100804-1.00006-2.

Xia, W., Huo, Y., Song, Y., Han, J., Dai, Y., 2019. Off-design analysis of a CO2 rankine cycle for the recovery of LNG cold energy with ambient air as heat source. Energy Convers. Manage. 183, 116–125. http://dx.doi.org/10.1016/j.enconman.2018.12.098.

Xiang, Y., Cai, L., Guan, Y., Liu, W., Han, Y., Liang, Y., 2019. Study on the integrated system of LNG oxy-fuel power plant and the application of supercritical CO2. Energy Procedia 158, 1863–1870. http://dx.doi.org/10.1016/j.egypro.2019.01.433.

Xiong, X., Lin, W., Gu, A., 2016. Design and optimization of offshore natural gas liquefaction processes adopting PLNG (pressurized liquefied natural gas) technology. J. Nat. Gas Sci. Eng. 30, 379–387. http://dx.doi.org/10.1016/j.jngse.2016.02.046.

Yang, J., Yang, Z., Duan, Y., 2020. Off-design performance of a supercritical CO2 Brayton cycle integrated with a solar power tower system. Energy 201, 117676. http://dx.doi.org/10.1016/j.energy.2020.117676.

Zaitsev, A., Mehrpooya, M., Ghorbani, B., Shermatov, R., Naumov, F., Shermatova, F., 2020. Novel integrated helium extraction and natural gas liquefaction process configurations using absorption refrigeration and waste heat. Int. J. Energy Res. 44, 1–22. http://dx.doi.org/10.1002/er.5377.

Zhang, N., Lior, N., Liu, M., Han, W., 2010. COOLCEP (cool clean efficient power): A novel CO2-capturing oxy-fuel power system with LNG (liquefied natural gas) coldness energy utilization. Energy 35, 1200–1210. http://dx.doi.org/10.1016/j.energy.2009.04.002.

Zhang, J., Meerman, H., Benders, R., Faaij, A., 2020. Comprehensive review of current natural gas liquefaction processes on technical and economic performance. Appl. Therm. Eng. 166, 114736. http://dx.doi.org/10.1016/j.applthermaleng.2019.114736.

Zhang, P., Saeid, M., 2022. Best practices in decarbonisation for LNG export facilities. Emiss. Reduct. 5–8, https://cdn.decarbonisationtechnology.com/data/articles/file/104-best-practices-in-decarbonization-for-GBPiquefied-naturaGBP-gas-export-faciGBPities-website.pdf.

Zhu, HH., Wang, K., He, YL., 2017. Thermodynamic analysis and comparison for different direct-heated supercritical CO2 Brayton cycles integrated into a solar thermal power tower system. Energy 140, 144–157. http://dx.doi.org/10.1016/j.energy.2017.08.067.